Biological Response to the Dynamic Spectral-Polarized Underwater Light Field

PI: Molly E. Cummings
Integrative Biology Department
University of Texas
Austin, TX 78712
phone: (512) 232-6243 fax: (512) 471-3878 email: mcummings@austin.utexas.edu
Co-PI: Samir Ahmed (City College of New York)
Co-PI: Heidi Dierssen (University of Connecticut)
Co-PI: Alexander Gilerson (City College of New York)
Co-PI: William F. Gilly (Stanford University)
Co-PI: George Kattawar (Texas A & M University)
Co-PI: Brad Seibel (University of Rhode Island)
Co-PI: James Sullivan (University of Rhode Island)

Award Number: N000140911054
http://www.bio.utexas.edu/research/cummingslab/

LONG-TERM GOALS

Camouflage in marine environments requires matching all of the background optical properties: spectral, intensity and polarization components─ all of which can change dynamically in space and time. Current research suggests that polarization detection is more sensitive than other conventional detection methods in scattering media such as the ocean, hence underscoring the need to develop polarized camouflage technology. Our research investigates the biological challenge of camouflage in the near-shore littoral zone and near-surface marine environments in two distinct water types found in coastal environments around the globe (oligotrophic and eutrophic) with particular emphasis on the polarization properties. We aim to characterize the dynamic light field along with the behavioral and cellular response of camouflaging animals in these environments. Our long-term goal is to identify the biological pathways for concealment against the underwater spectral-polarized light field enabling us to identify design principles for future naval camouflage.

OBJECTIVES

(1) Measure and model the spectral-polarized light field in near-shore and near-surface environments

(2) Characterize the biological camouflage response of organisms to these dynamic optical fields

(3) Identify the internal controls and structural mechanisms that coordinate the camouflage response

APPROACH

Our first aim is to **measure and model the underwater spectral-polarized light field in distinct water types**. We characterize the light field by the simultaneous deployment of a comprehensive

Report Documentation Page

Form Approved
OMB No. 0704-0188

1. REPORT DATE	2. REPORT TYPE	3. DATES COVERED
30 SEP 2013		**00-00-2013 to 00-00-2013**

4. TITLE AND SUBTITLE	5a. CONTRACT NUMBER
Biological Response to the Dynamic Spectral-Polarized Underwater Light Field	5b. GRANT NUMBER
	5c. PROGRAM ELEMENT NUMBER
6. AUTHOR(S)	5d. PROJECT NUMBER
	5e. TASK NUMBER
	5f. WORK UNIT NUMBER
7. PERFORMING ORGANIZATION NAME(S) AND ADDRESS(ES) **University of Texas,Integrative Biology Department,Austin,TX,78712**	8. PERFORMING ORGANIZATION REPORT NUMBER
9. SPONSORING/MONITORING AGENCY NAME(S) AND ADDRESS(ES)	10. SPONSOR/MONITOR'S ACRONYM(S)
	11. SPONSOR/MONITOR'S REPORT NUMBER(S)

12. DISTRIBUTION/AVAILABILITY STATEMENT
Approved for public release; distribution unlimited

13. SUPPLEMENTARY NOTES

14. ABSTRACT

15. SUBJECT TERMS

16. SECURITY CLASSIFICATION OF:			17. LIMITATION OF ABSTRACT	18. NUMBER OF PAGES	19a. NAME OF RESPONSIBLE PERSON
a. REPORT	b. ABSTRACT	c. THIS PAGE			
unclassified	**unclassified**	**unclassified**	**Same as Report (SAR)**	**40**	

optical suite including underwater video-polarimetry (full Stokes vector video-imaging camera custom-built Cummings; and "SALSA" (Bossa Nova Technologies, CA) Gilerson), inherent optical properties, (LISST by Dierssen), hyper-spectral multi-angular Stokes vector spectroradiometry (Gilerson,Ahmed), and the volume scattering function measures (MASCOT by Sullivan). These measurements will be used to refine development of, and make comparisons to, theoretical expectations from a fully 3-D radiative transfer model that solves for each of the polarization elements of the Mueller matrix transformation of the Stokes vector by (Kattawar). The first modeling objective of this proposal is to calculate the complete Mueller matrix/Stokes vector for any set of oceanic and atmospheric conditions for any region of the ocean. We will then use this modeling approach (*i*) to predict the 3-D light field; (*ii*) to calculate experimental conditions to measure biological responses; and (*iii*) to investigate the nature of the light field as it interacts with cells within the skin. Our approach is to develop a 3-D Monte Carlo model with full Mueller matrix treatment.

During field operations, we couple polarimetry measurements of live, free-swimming animals in their environments with a full suite of optical measurements (mentioned above) to completely characterize the **biological response to dynamic optical environments** (Cummings, Gilerson, Dierssen, Sullivan, Seibel, Ahmed)**.** We also restrain live, awake animals to take polarimetry measurements (in the field and laboratory) under a complete set of viewing angles and incident polarization light fields. We use Mueller matrix modeling to determine the specific Mueller matrix elements of animals that differ from those of conventional structures currently deployed for open ocean camoflauge (e.g. standard mirror). Furthermore, we examine *in vivo* "flickering" activity on the skin of several species of squid and its relationship to background matching (wave-induced fluctuations of the light field) (Gilly).

We **identify the internal control of these field-studied organisms and structural mechanisms that coordinate the camouflage response** by (a) characterizing different tissue layers and organelles associated with different species occupying a diverse array of marine habitats using a combination of light and SEM microscopy (Cummings, Gilly), (b) examining both iridophore and chromatophore control processes and the local vs peripheral control features using both pharmacological and electrical stimulation techniques (Gilly, Cummings), and (c) developing a novel 3D Monte Carlo model to describe how the spectral-polarized light field interacts with cells within the skin (Kattawar).

WORK COMPLETED

a) Presented at Ocean Optics in October 2012 (Dierssen, Sullivan, Gilerson,Cummings, Kattawar).

b) Participated in annual MURI group meeting field planning meeting Oct 2012 (Cummings, Dierssen, Sullivan, Gilerson, collaborator Twardowski)

c) Completed and submitted paper on bio-mimicry model for Polaro-cryptic mirror based on the lookdown, Selene vomer (Cummings)

d) Completed data analysis of 2012 Field Campaign in Curacao for field test of polaro-cryptic model with new open ocean fish species including optical measurements: spectral stokes vector radiometery, polarization videoimagery, IOPs and VSF, partical size distributions, remote sensing reflectance, benthic reflectance spectrometry, and sensor packages providing measurements of fish, camera and sun orientation (Cummings, Gilerson, Sullivan, Dierssen, Twardowski)

e) Completed and submitted Group paper combining data and simulation using a vector radiative (RT) transfer code from two 2011 field campaigns that measured polarization characteristics of

shallow water environments with diverse substrates. (Gilerson, Ahmed, Sullivan, Twardowski, Dierssen, Cummings)

f) Completed and submitted group paper examining the biological structural mechanisms of polaro-crypsis and broadband reflectance in the Lookdown, *Selene vomer*. (Cummings, Kattawar)

g) Completed analysis and submitted paper examining differences in polarization reflectance between species of different optical habitats, and peripheral vs central control of polarization reflectance. (Cummings)

h) Completed and published paper examing the extinction properties of the layered structure of cephalopod iridosomes (Kattawar)

i) Completed and published paper combining data and simulation examing the broadband reflectance of leucophores in the cuttlefish, *Sepia officinalis* (Kattawar)

j) Completed and published paper proposing a novel Muller matrix holography method to characterize the structure and composition of small particles, such as leucosomes and iridosomes. (Kattawar)

k) Completed and published paper examining the intrinsic angular properties of diffuse reflectance (Kattawar)

l) Completed and published paper proposing a new method to detect and monitor dinoflagellates such as K. brevis, the causal agent of the Florida red tide. (Kattawar)

m) Completed and submitted paper generalizing the conventional Lorenz-Mie theory for a case when the light source is partially spatially coherent. (Kattawar)

n) Wrote program following Sutherland (Sutherland RL, Mäthger LM, Hanlon RT, Urbas AM, Stone MO.J Opt Soc Am A ,Opt Image Sci Vis. 2008 Mar; 25(3):588-99.*)* model. (Kattawar)

o) Modified Mie Code (Absorption and Scattering of Light by Small Particles" by Bohren, Craig F., Huffman, Donald R, 1983, Wiley, New York) to find an index of refraction of a pigment granule, that, when inserted into an ellipsoid filled with spheres (model of a chromatophore) matches the backscattering and absorption cross sections produced by the Sutherland program. Some of these parameters are still being adjusted to make a better match. (Kattawar)

p) Data from previously measured polarization characteristics of light in shallow waters environments with seagrass, coral reef and sand bottoms (Florida Keys, January and August 2011) were analyzed together with simulations obtained using a vector radiative (RT) transfer code RayXP. Group paper is submitted to Applied Optics. (Gilerson)

q) Development of the model for polarized imaging of the target and comparison with experiments in clear waters (Curacao, 2012) and coastal waters (NY Bight, 2012). Algorithm is proposed for the restoration of the targets polarization properties from the full Stokes vector image made by video-imaging camera “SALSA” (Bossa Nova Technologies, CA). (Gilerson)

r) Recently developed polarization technique for the retrieval of the attenuation/absorption ratio of water from the polarized measurements for coastal waters is extended and analyzed for open ocean water conditions. (Gilerson)

s) Field experiments in Chesapeake Bay (August 2013) for polarization imaging of the target with various polarization features together with measurements of water inherent optical properties and polarization characteristics of light by the polarimeter in various water environments, illumination and viewing conditions. Data are being processed for the further model and algorithm development. (Gilerson)

t) Completed field work in Sargasso Sea aboard the R/V Sea Dragon measuring camouflage in two different species of crab living in floating mats of the brown algae *Sargassum* using hyperspectral imaging techniques. Project included outreach, education, and conservation work with Bermuda environmental organizations and our research was featured in the Bermuda Royal Gazette (Dierssen).

u) Conducted laboratory experiments using hyperspectral imaging of juvenile intertidal crab species *Hemigrapsus sanguineus*, *Carcinus maenas*, and *Panopeus herbstii* in relationship to their habitats (Dierssen).

v) Developed a new underwater housing and control system for the custom-built dive spectrometer to make benthic reflectance measurements (Dierssen).

w) We developed a Matlab-based software platform and graphical user interface (Squid Skin GUI) to permit automated analysis of Crittercam video data (Gilly).

RESULTS

1. The polarized extinction properties of iridosome plates are obtained. Agreement is found between the results for the infinite-radius plates and plates with large aspect ratios and small incident angles (Fig. 1). The connection between these two cases provides a basis into the understanding of the extinction properties of non- spherical particles illuminated by polarized incident light.
2. The broad band reflectance of cuttlefish leudophores is simulated using a radiative transfer code, and is compared with measurements (Fig. 2). The agreement between simulation and data suggests the broad band reflectacance is produced by incoherent multiple scattering.
3. The Mueller matrix formalism is introduced into the holography method. It is found that the conventioanl method which excludes polarization information cannot characterize small anisotropic particles, but the new method provides such a capability and can be useful for the study of small biological structures (Fig 3).
4. The angular distribution of diffuse reflection is elucidated with greater understanding by studying a homogeneous turbid medium. The diffuse reflection is produced by incoherent multiple scattering and is solved through radiative transfer theory. Specific angular distributions of the reflectance are found related to the system optical depth, incident angle, and the assymetry factor, and thus provide a relevant reference for the study of the reflectance properties of biological systems (Fig 4).
5. The nucleus of a dinoflagellate is modeled and the Mueller matrix of light scattering is simualted using the DDA code. The results show strong S_{14} back scattering signals when the wavelength of incdient light matches the pitch of the chromosomes (Fig.5).
6. The conventional Lorenz-Mie theory is generalized to a case when the light source is partially coherent. The influence of the degree of coherence of the incident field on the Mueller matrix is studied analytically. The formailism is applied to cases of large spherical droplets in water clouds and hexagonal ice crystals in cirrus clouds. The results show some Mueller matrix elements, such as S_{22}, depend monotonically on the coherence length of the incident beam (Fig. 6, 7), which provides a promising method to measure the degree of coherence.
7. Reflectance and transmittance can be generated from the calculated index of refraction of the pigment granules. Although some minor adjustments must still be made, with a correct index of refraction, we can simulate a yellow chromatophore of any size. The same method can also be

applied to any other color chromatophore to find an index of refraction of the pigment granules and make a simulation of that chromatophore as well. See Figs. 8-14

8. Hyperspectral polarization measurements in shallow waters show that in most cases a Lambertian unpolarized bottom with proper spectral reflectance represents an appropriate model to determine polarization characteristics of light in the water column. Correlation between measured and simulated degree of linear polarization DoLP at one of the stations is shown in Fig. 15, measured and simulated DoLP at 440nm for all stations – in Fig. 16. Whereas the DoLP is highly sensitive to benthic reflectance, the angle of polarization (AoLP), which quantifies the orientation of polarization, is independent of it. The AoLP could therefore be used to communicate and sense direction underwater (paper submitted).
9. Full Stokes vector images and video of targets with various polarization shown that even in clear water the impact of the water body on the polarized underwater image is very significant and retrieval of target polarization characteristics from the image is extremely challenging. (Fig 17,18)
10. Extensive simulations of polarization characteristics of light in a broad range of water environments based on the open ocean model (RayXP code) found that the retrieval of the attenuation/absorption ratio of water from the polarized measurements of water leaving radiance has its highest sensitivity around 550nm while in coastal waters 440 nm and 665 nm were more favorable for the retrieval.
11. Technology for conducting airborne and underwater hyperspectral imaging developed through this project has led to development and testing of new sensors and techniques for conducting habitat mapping of optically shallow habitats such as seagrass as well as deep seafloors.
12. Using hyperspectral imaging, excellent color matching was observed between *Sargassum* seaweed and both endemic crab species across the visible wavelengths except in the chlorophyll absorption band at 676 nm. Specific components of crab coloration was found to closely match spectral reflectance of elements in habitat (barnacles, healthy and senescent algae, etc.) (Fig. 19).
13. Some species can camouflage across the entire visible spectrum including the chlorophyll absorption band. The sea hare *Phyllaplysia taylori* shows close spectral matching to its seagrass habitat and has elements that match both living and senescent seagrass (Fig.20)
14. Sargassum crab *Portunus sayi* can dynamically camouflage in response to diel light cycles and its background habitat through the use of chromatophores beneath the transparent carapace (Fig. 21).
15. The peer reviewed article in PNAS shows a model for polarization camouflage for fish in the open ocean incorporating both measurements of the polarization reflections of fish and models of the predicted polarization contrast minimization. (Fig 22).
16. We identified four types of guanine platelets (Types 1-4) in the lookdown skin with a specific arrangement that can produce broadband reflection (Fig 23,24) as well as adaptive birefringence enabling polaro-crypsis in an open ocean environment (Fig 25).
17. Fish occupying different optical habitats (in terms of polarization features) exhibit statistically distinct polarization reflectance (Fig 26,27).
18. Lab polarization manipulation experiments revealed that polarization reflectance in Atlantic needlefish is controlled at the periphery (Fig 28).

19. Quantitave analysis of the skin optical properties of live squid coupled with the optical properties of the water column has allowed us to determine whether the 'flickering' and 'flashes' of the humboldt squid represents a dynamic camouflage strategy (Figs 29-31).
20. Pharmacological testing of sodium channels in squid nerve fibers confirmed our hypothesis for peripheral control of chromatophore activity (Fig 32-34)
21. Inherent optical properties, including polarized elements of the VSF, of the 2012 field campaign in Curacao were found to be relatively consistent (varying in 15-20% in magnitude, Fig 35). These results are bing used as part of a larger analysis in understanding how particle fields affect in situ polarization, and will be the first attempt in explaining variability in polarization elements in terms of the natural particle field composition (Fig 36).

IMPACT/APPLICATIONS

Polarized scattering measurements can be used to predict and optimize the performance of a host of Naval operations that rely on laser imaging systems, laser communications, cameras, and other active and passive remote sensing systems.

Biological strategies for polaro-crypsis may be adopted for technological and military applications addressing the need to minimize object detection in open ocean conditions.

RELATED PROJECTS

The CCNY group also studied polarization characteristics of light in water through another award from ONR N00014-10-1-0368 (2009-12, extended for 2013)

Results of our hyperspectral imaging has lead to UCONN becoming a partner in the proposed new Centre for research-based innovation (SFI): Centre for Ocean Observation Applications - COOA led by the Norwegian University of Science and Technology (NTNU) and including large industries such as Statoil, ENI, DNV, KM. The intent is to build an international leading centre for innovation driven research bridging technology and natural science for multidisciplinary theoretical and experimental research using autonomous airborne and underwater robotics and sensors for bio-geo-chemical ocean observation. To meet the challenges in Norwegian and Arctic waters related to oil and gas industry, marine mineral mining, fisheries and new transport routes will include new techniques for identification, mapping and monitoring of the marine environment. (Dierssen)

Establishing collaborations with camouflage researchers on isopod and kelp crab camouflage against algae and seagrasses at several different west coast universities (Dierssen).

Research on camouflage featured on the technology company Surface Optics website:
http://surfaceoptics.com/soc710-aboard-sea-dragon-research-vessel/
(Dierssen)

Submitted proposals to National Geographic Society for additional Crittercam deployments on Humboldt squid: "Natural behaviors of Humboldt squid in relation to oxygen-limited habitats; PI Gilly, $25,000 direct costs, awarded) and "Natural behaviors of free-swimming *Dosidicus gigas* studied with an animal-born-video package and data-loggers; Young Explorer Program, PI Rosen, $4,675 direct costs, pending).

Submitted a proposal to NSF in collaboration with National Geographic Remote Imaging to develop a low-light, high-speed, HD Crittercam and midwater Driftcam system and to use both systems to study natural chromogenic behaviors of Humboldt squid. This proposal continues the laboratory work (physiology and immunohistochemistry) that was initiated during this award. PI Gilly, $635,996 direct costs, pending.

In line with our goal of understanding how different particle fields affect in-situ inherent optical properties (e.g. polarized scattering elements and spectral backscattering), Sullivan and Twardowski have been developing an in-situ holographic microscope (HOLOCAM) capable of characterizing the properties of particles within a size range of < 1 μm to > 1 mm in an undisturbed volume of water (ONR NOPP project N0001410C0041). This system has now been built and field tested and will be used in any future MURI field effort to better link the natural particle fields to the resultant optics.

PUBLICATIONS

Brady P, Travis K, Maginnis T, **Cummings** ME (2013) The polaro-cryptic mirror: a biological adaptation for open-ocean camouflage. *Proceedings of the National Academy of Sciences,* 110: 9764-9769 [published, refereed].

Zhao S, Brady P, Gao M, Etheredge I, **Kattawar** GW, **Cummings** ME (2013) Characterization of broadband and polarization reflectors in the lookdown, *Selene vomer*. *Proceedings of the Royal Society of London A*.

Ruddick KR, Brady P, Gruev P, **Cummings** ME (2013) Polarized reflectance of marine fish from different habitats- an examination of habitat-dependent polaro-crypsis and central versus peripheral control. *Journal of Experimental Biology.*

Calabrese G, Brady P, Gruev V, **Cummings** ME. (2013). Dynamic polarization signaling in swordtails alters female mate preference. *Proceedings of the National Academy of Sciences.*

Gao M, You Y, Yang P, and **Kattawar** GW (2012) Backscattering properties of small layered plates: a model for iridosomes. *Optics Express*, 20, 25111-25120 [published, refereed].

Gao M, Yang P, **Kattawar** GW (2013) Polarized extinction properties for plates with large aspect ratios. *Journal of Quantitative Spectroscopy and Radiative Transfer* [in press, refereed].

Mäthger LM, Senft SL, Gao M, Karaveli S, Bell GRR, Zia R, Kuzirian AM, Dennis PB, Crookes-Goodson WJ, Naik RR, **Kattawar** GW, Hanlon RT (2013) Bright white scattering from protein spheres in color changing, flexible cuttlefish skin. *Advanced Functional Materials*, **23**, 3980–3989 [published, refereed].

Gao M, Yang P, McKee D, **Kattawar** GW (2013) A Mueller matrix holographic method for small particle characterization: theory and numerical studies. *Applied Optics* 52, 5289-5296 [published, refereed].

Gao M, Huang X, Yang P, **Kattawar** GW (2013) Angular Distribution of Diffuse Reflectance from Incoherent Multiple Scattering in Turbid Media. *Applied Optics* 52, 5869–5879 [published, refereed].

Liu J, **Kattawar** GW (2013) Detection of dinoflagellates by the light scattering properties of the chiral structure of their chromosomes. *Journal of Quantitative Spectroscopy and Radiative Transfer*, 20, 25111-25120 [published, refereed].

Liu J, Lei B, Yang P, **Kattawar** GW (2013) Scattering of partially coherent electromagnetic beams by water droplets and ice crystals. *Journal of Quantitative Spectroscopy and Radiative Transfe.r*

Gilerson AA, Stepinski J, Ibrahim AI, You Y, **Sullivan** JM, **Twardowski** MS, **Dierssen** HM, Russell B, **Cummings** ME, Brady P, **Ahmed** SA, and **Kattawar** GW (2013) Benthic effects on the polarization of light in shallow waters. *Applied Optics*.

Harmel T, **Gilerson** A, Tonizzo A, Chowdhary J, Weidemann A, Arnone R, **Ahmed** S (2012) Polarization impacts on the water-leaving radiance retrieval from above-water radiometric measurements. *Applied Optics*, 51, 8324-8340 [published, refereed].

Ibrahim A, **Gilerson** A, Harmel T, Tonizzo A, Chowdhary J, **Ahmed** S (2012) The relationship between upwelling underwater polarization and attenuation/absorption ratio. *Optics Express*, 20, 25662-25680 [published, refereed].

Ibrahim A, **Gilerson** A, Stepinski J, El-Habashi A, **Ahmed** S (2013) The retrieval of scattering coefficient of marine particles from polarimetric observations. *Proc. of SPIE*, 8873 [published].

Gilerson A, Carrizo C, Tonizzo A, Ibrahim A, El-Habashi A, Foster R, **Ahmed** S (2013) Polarimetric imaging of underwater targets. *Proc. of SPIE*, 8724 Security and Defense [published].

Ahmed S, Tonnizo A, Ibrahim A, **Gilerson** S, Gross BM, Moshary F (2012) Algal fluorescence in coastal waters: impact and potential for retrieval from measurements of the underwater degree of polarization. *Proc. of SPIE*, 8532 Remote Sensing of the Ocean, Sea Ice, Coastal Waters, and Large Water Regions [published].

Pettersen R, Johnsen G, Bruehim P, Volent Z, **Dierssen** HM (2013) Bio-optical properties of the deep water coral *Lophelia pertusa* pigment signatures using hyperspectral imaging in laboratory and underwater. *Appl. Optics*. [published, refereed].

Mouroulis P, Gorp BV, Green R, **Dierssen** HM, Wilson DW, Eastwood M, Boardman J, Gao B, Cohen D, Franklin B, Loya F, Lundeen S, Mazer A, McCubbin I, Randall D, Richardson B, Rodriguez JI ,Sarture C, Urquiza E, Vargas R, White V, Yee K (2013) The Portable Remote Imaging Spectrometer (PRISM) coastal ocean sensor: characteristics and first flight results. *Appl. Optics*. [published, refereed].

Hill V, Zimmerman RC, Bissett WP, Kohler DDR, **Dierssen** HM (revision) Evaluating light availability and seagrass biomass and productivity using hyperspectral airborne remote sensing in Saint Joseph's Bay, Florida. *Estuaries and Coasts*.

Bostrom K, **Dierssen** HM (revision) Hyperspectral Airborne Remote Sensing of Eelgrass in the Turbid Waters of Elkhorn Slough, California. *IEEE Journal of Selected Topics in Applied Earth Observations and Remote Sensing* (JSTARS).

Johnsen G, Volent Z, **Dierssen** HM, Pettersen R, Ardelan MV, Søreide F, Fearns P, Ludvigsen M, Moline M (2013) Underwater hyperspectral imagery to create biogeochemical maps of seafloor properties. *Subsea Optics and Imaging*. Ed. J. Watson and O. Zielinski. [in press, refereed]

Dierssen HM, Randolph K **(**2013) Remote Sensing of Ocean Color. *Encyclopedia of Sustainability Science and Technology*. Springer-Verlag Berlin Heidelberg. 25 pp. http://www.springerreference.com/index/chapterdbid/310809 [published, refereed]

Heupel E, **Dierssen** HM, Gao B, Green RO, Mouroulis P (2013) Hyperspectral Remote Sensing in Coastal Regions: PRISM Field Validation in Elkhorn Slough. *Workshop on Hyperspectral Image*

and Signal Processing : Evolution in Remote Sensing (WHISPERS - www.ieee-whispers.com) IEEE [in press, refereed].

Dierssen, H.M. Accepted. Overview of hyperspectral remote sensing for mapping marine benthic habitats from airborne and underwater sensors. Proceedings of SPIE Imaging Spectrometry XVIII. San Diego, CA September, 2013 [in press].

Gilly WF, Beman JMB, Litvin SY, Robison BH (2013) Oceanographic and Biological Effects of Shoaling of the Oxygen Minimum Zone. *Annual Rev. Marine Sci.* 5: 393–420 [published].

Hoving H-J, **Gilly** WF, Markaida U, Benoit-Bird KJ, West-Brown Z, Daniel P, Field JC, Parassenti L, Liu B, Campos B (2013) Extreme plasticity in life-history strategy allows a migratory predator (*Dosidicus gigas*) to cope with a changing climate. *Global Change Biology* 19*:*2089 –2103 [published]**.**

Stewart J, Field JC, Markaida U, **Gilly** WF (2013) Behavioral ecology of jumbo squid (*Dosidicus gigas*) in relation to oxygen minimum zones. *Deep Sea Research II* [in press].

Stewart JS, Hazen EL, Bograd SJ, Byrnes JEK, Foley DG, **Gilly** WF, Robison BH, Field JC (2013) Combined climate- and prey-mediated range expansion of Humboldt squid (*Dosidicus gigas*), a large marine predator in the California Current System. *Global Change Biology*.

Staaf DJ, **Gilly** WF, Denny MW (2013) Aperture effects in squid propulsion**.** *Journal of Experimental Biology*.

HONORS/AWARDS/PRIZES

Heidi M. Dierssen, University of Connecticut (UCONN), was elected to be a member of the International Ocean Colour Coordinating Group (IOCCG) . This is an international Committee of experts comprising representatives from both the provider (Space Agencies) and user communities (scientists, managers) to develop consensus and synthesis at the world scale in the subject area of satellite ocean colour radiometry (OCR). http://www.ioccg.org/about/members.html

Molly Cummings, received the "*2012 Women in Science*" award by Indiana State University.

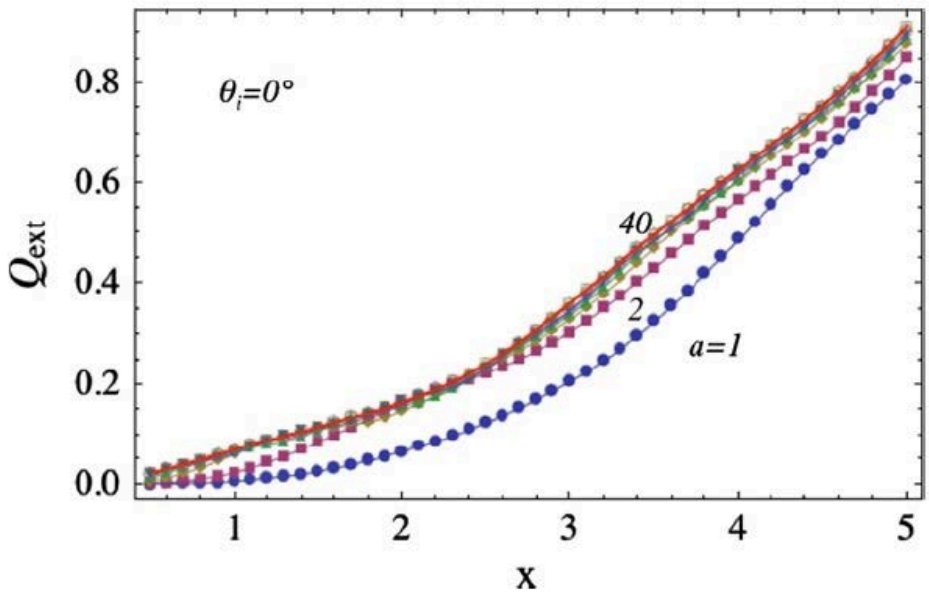

Fig. 1. Extinction efficiency Q_{ext} versus size parameter x with different aspect ratios: a=1, 2, 4, 6, 8, 10, 20, and 40 at incident angle θ_i=0. The extinction efficiency results for a=4, 6, 8, 10, 20, and 40 almost overlap each other. The solid red line is the infinite-radius plate results at normal incidence.

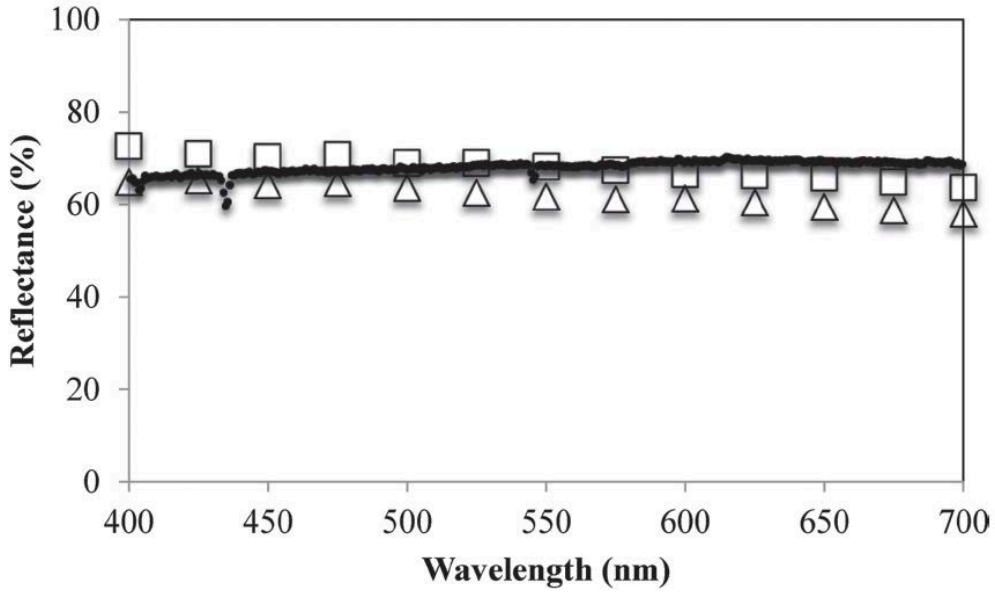

Fig. 2. Simulations show that the cuttlefish fin spot system approximates a Lambertian surface. Dots: Measured reflectance (from 400–700 nm) from cuttlefish fin spot can be as high as ca. 70%, reflecting equally well across the visible spectrum. Triangles: modeled flux reflectance spectrum averaged over all reflection angles and for 0 degree incidence. Squares: the normalized reflectance spectrum obtained by normalizing the modeled reflectance to a perfect Lambertian reflector at the same 0 degree incident and reflection angle, which is commensurate with the measurement. The normalized reflectance averaged over the visible spectrum is chosen to be the same as the measurement (both are 68%).

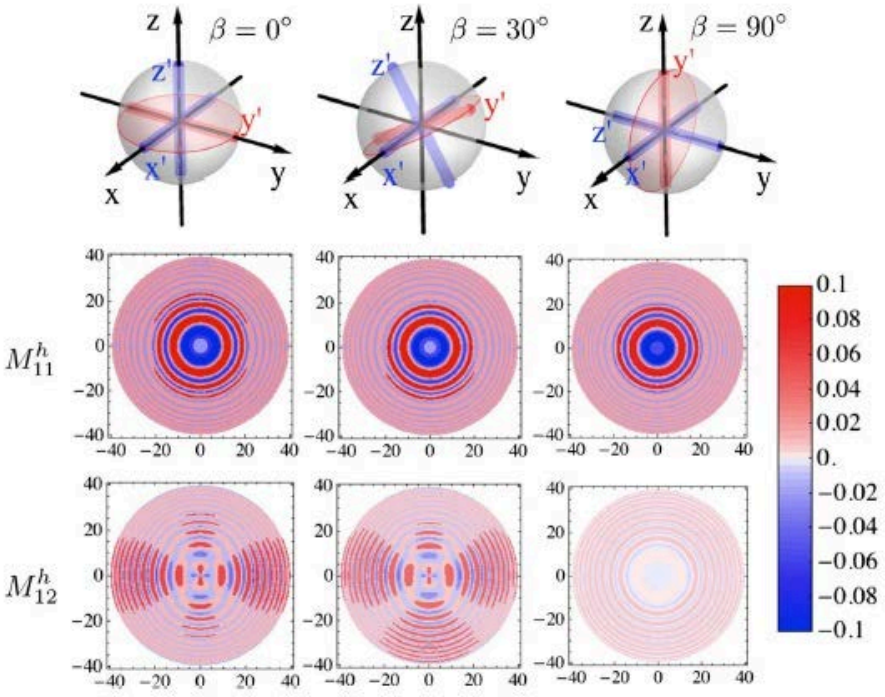

Fig. 3. The angular distribution of holographic Mueller matrix elements M^h_{11} and M^h_{12} for a birefringent sphere (refractive indices n_x=n_z= 1.7 and n_y=1.9) with size parameter ka =5 and orientation β =0°, 30°, and 90°. The polarization element M^h_{12} is sensitive to the particle orientations compared with the intensity element M^h_{11} typically available through the conventional holographic method.

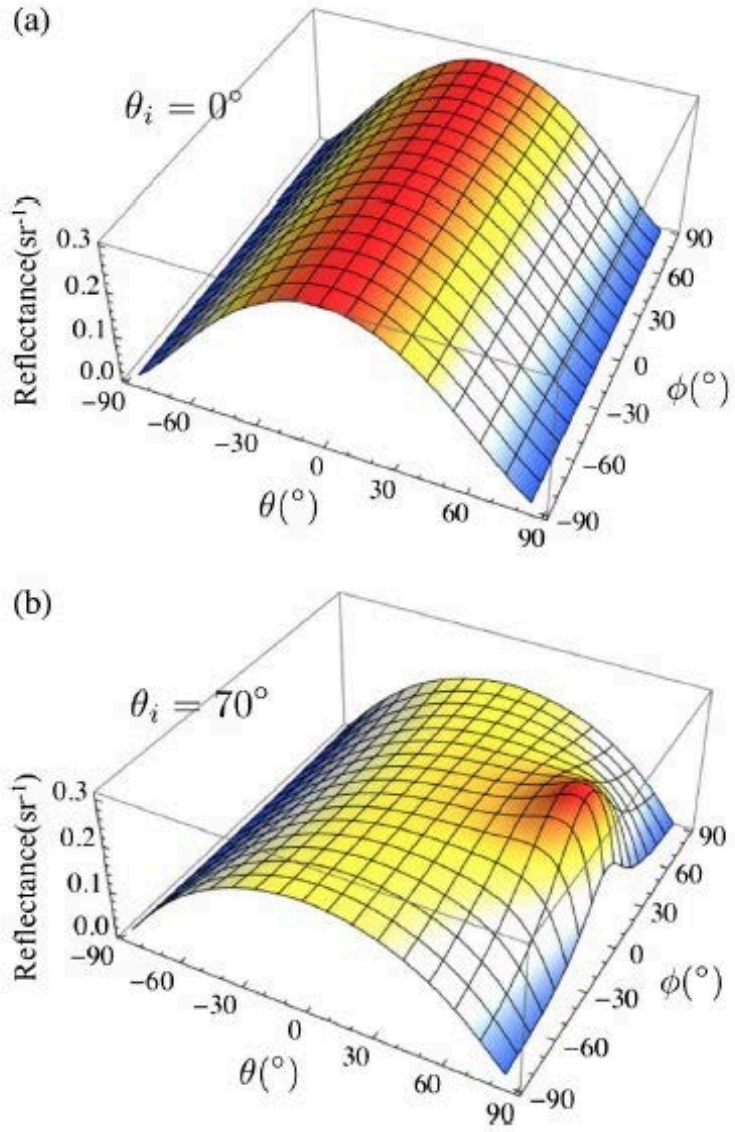

Fig. 4. Angular reflectance versus both zenith angle θ and azimuthal angle ϕ. The system has an adjusted optical depth τ= 10, asymmetry factor g =0.9, and incident angle (a) θ_i= 0° and (b) θ_i = 70°. The maximum reflection angle shown in (b) can be used to characterize the overall angular distribution of the reflectance, and is sensitive to the system optical depth, incident angle, and asymetry factors.

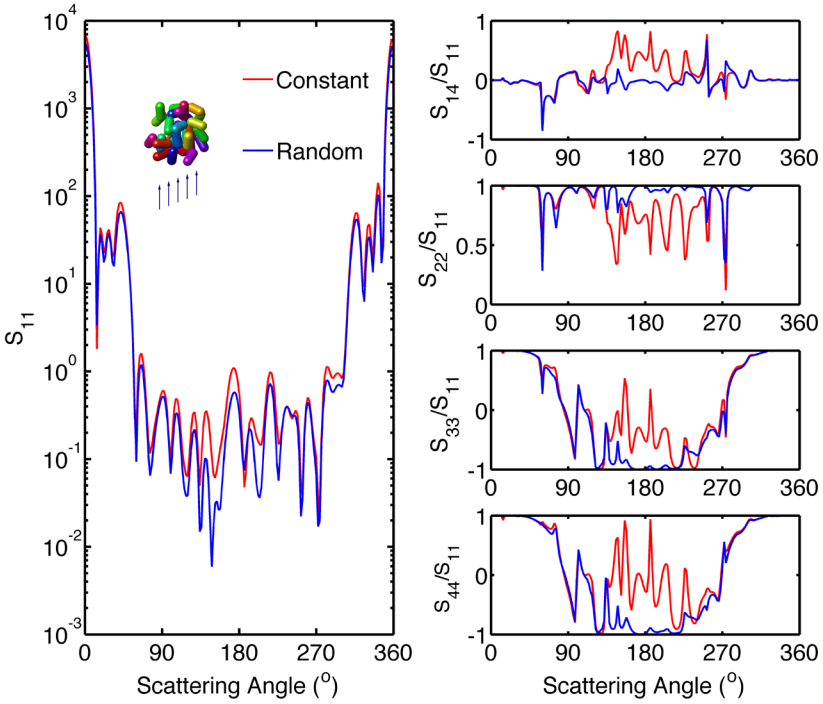

Fig. 5. Mueller matrix elements of a fixed dinoflagellate calculated using the nucleus model and the simplified chromosome model. The red line is the case when the twist angle is 45°, while the blue line is the one with random twist angle in each layer. In both cases, the light wavelength is 0.5 μm, which matches the pitch of the helical structure. The nucleus has diameter 4.0 μm. The chromosome has diameter 0.5 μm, length 1.0 μm and pitch 0.5 μm. The refractive index used is 1.2+0.01i and the scattering plane is yz plane.

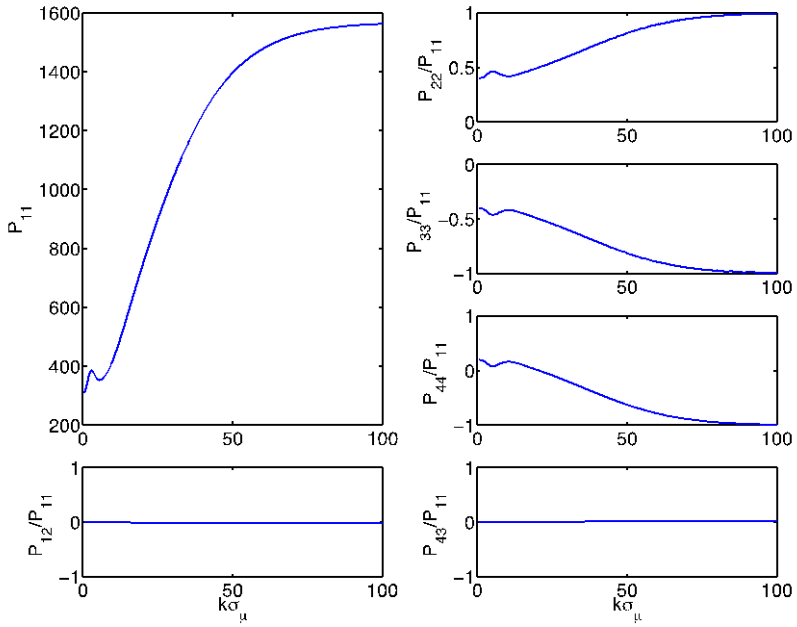

Fig. 6. Mueller matrix elements for a water droplet in the backward direction (180°). The coherence length parameter $k\sigma_\mu$ is from 0 to 100. The size parameter of the water droplet is $x = 80$ and the refractive index is $n = 1.33$.

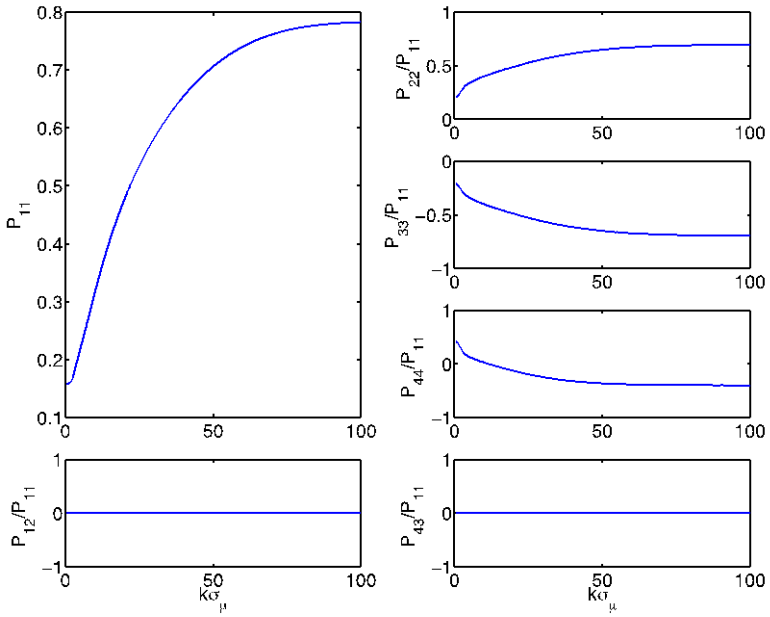

Fig. 7. Mueller matrix elements for a hexagonal ice crystal in the backward direction (180°). The coherence length parameter $k\sigma_\mu$ is from 0 to 100. The hexagonal ice crystal has size parameter $kL = 2ka = 150$, where L is the height and a is the semi-width, and refractive index $n = 1.31$.

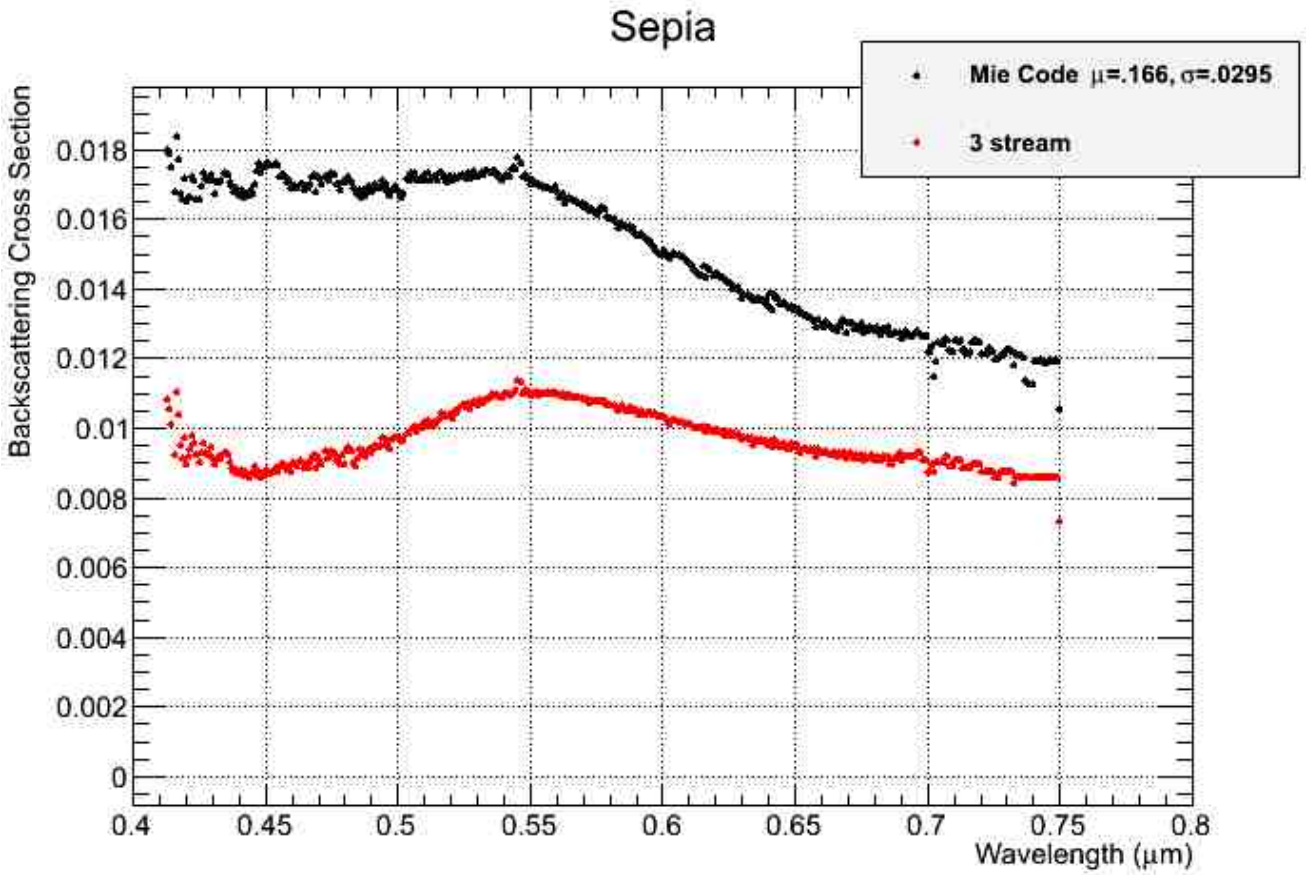

Fig. 8. The backscattering cross section now has the correct shape.

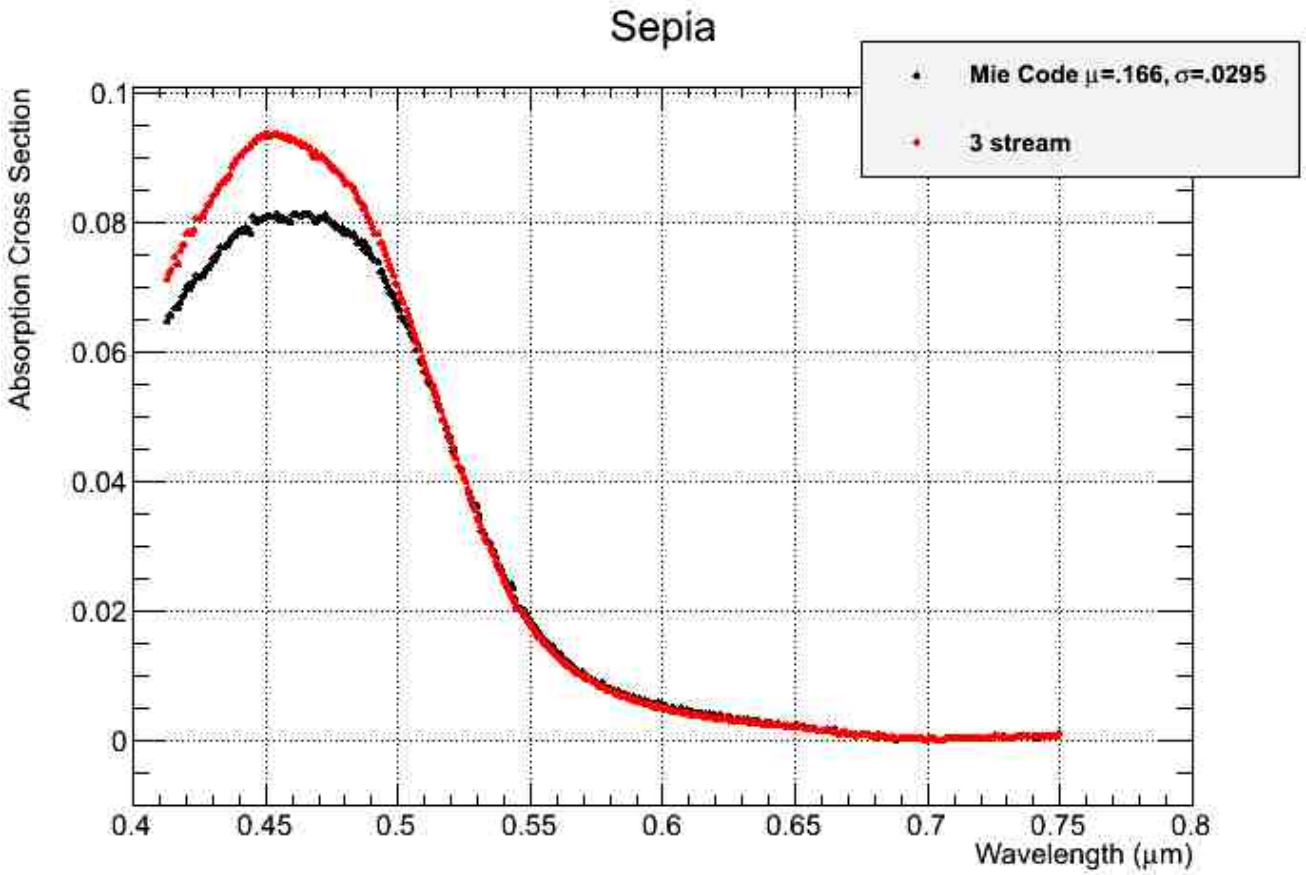

Fig. 9 The absorption correction matches well except for in the lower wavelengths.

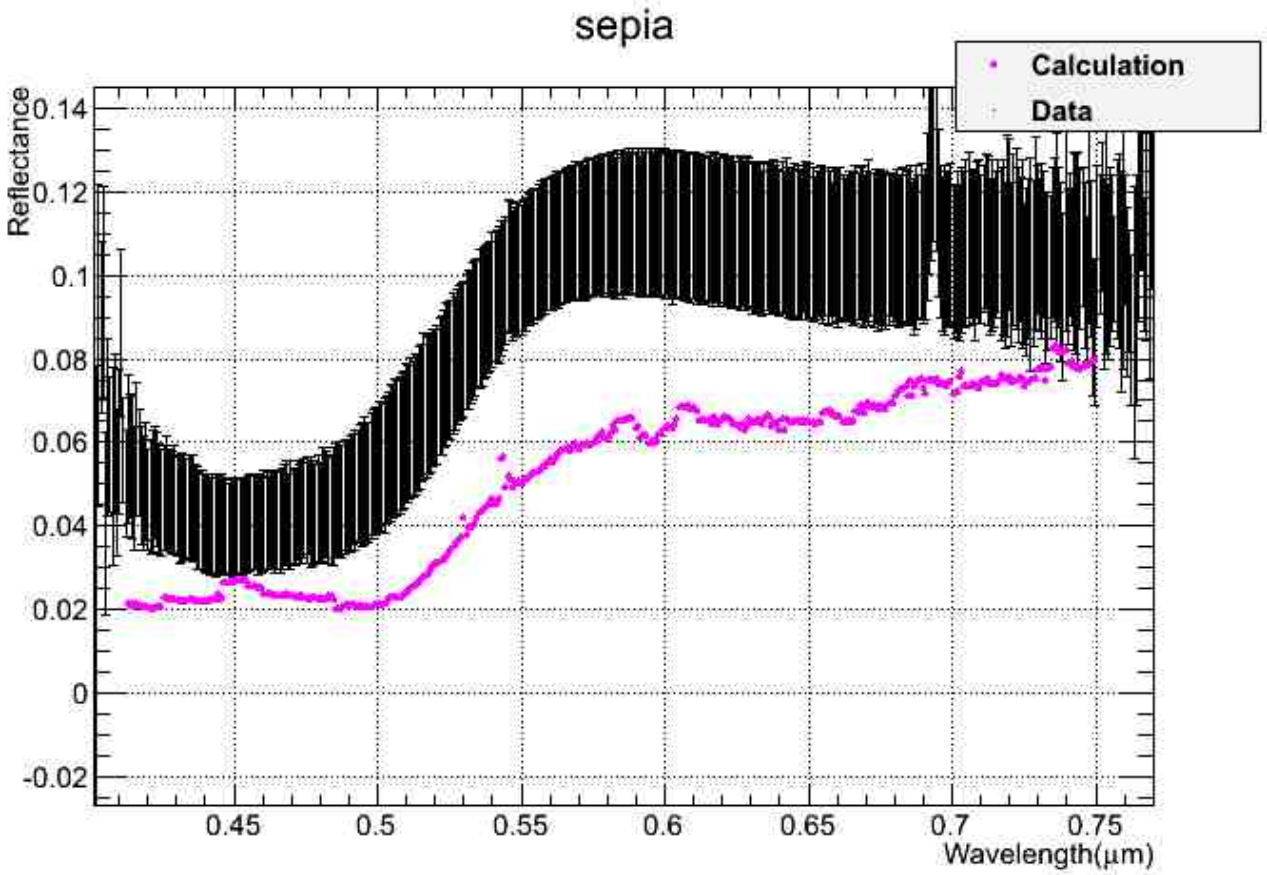

Fig. 10 Reflectance.

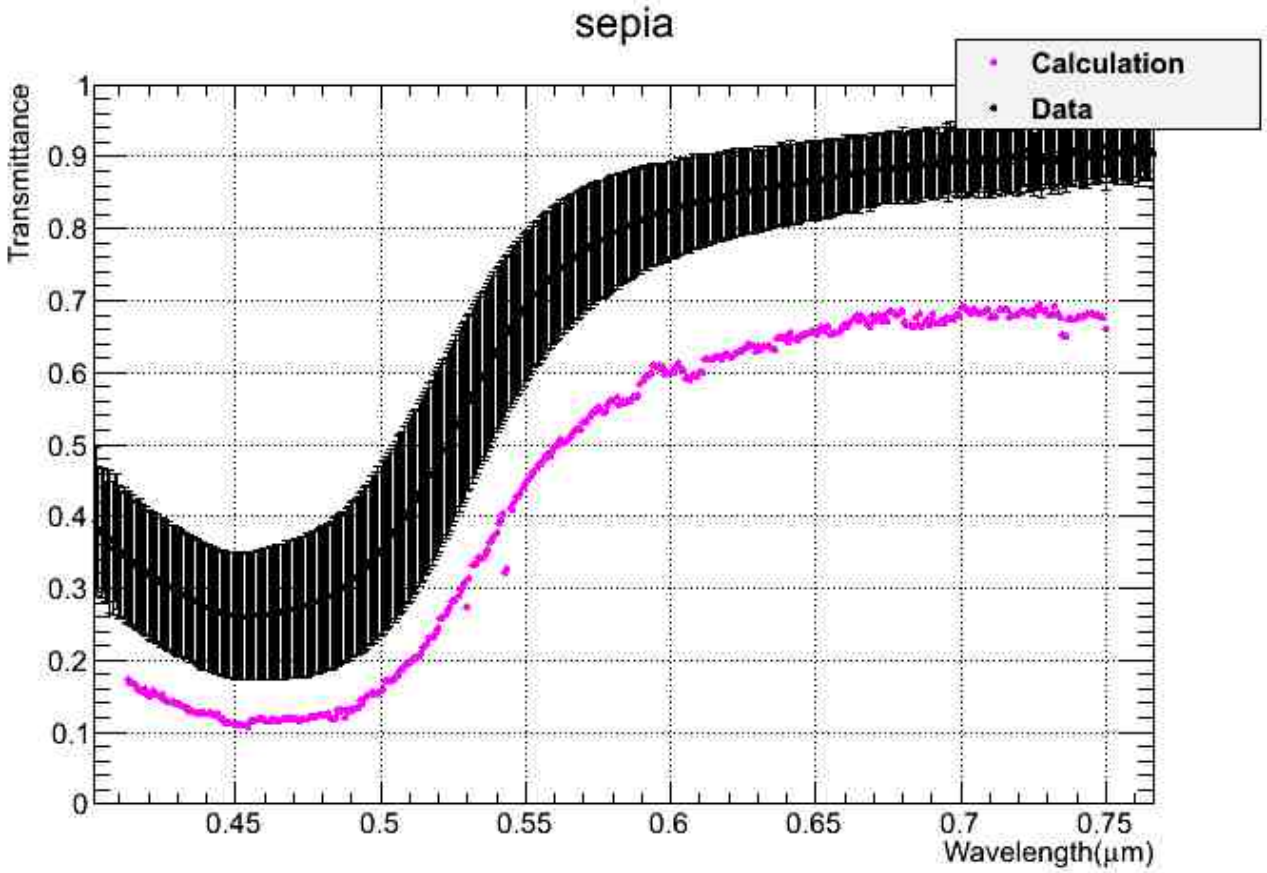

Fig. 11 Transmittance

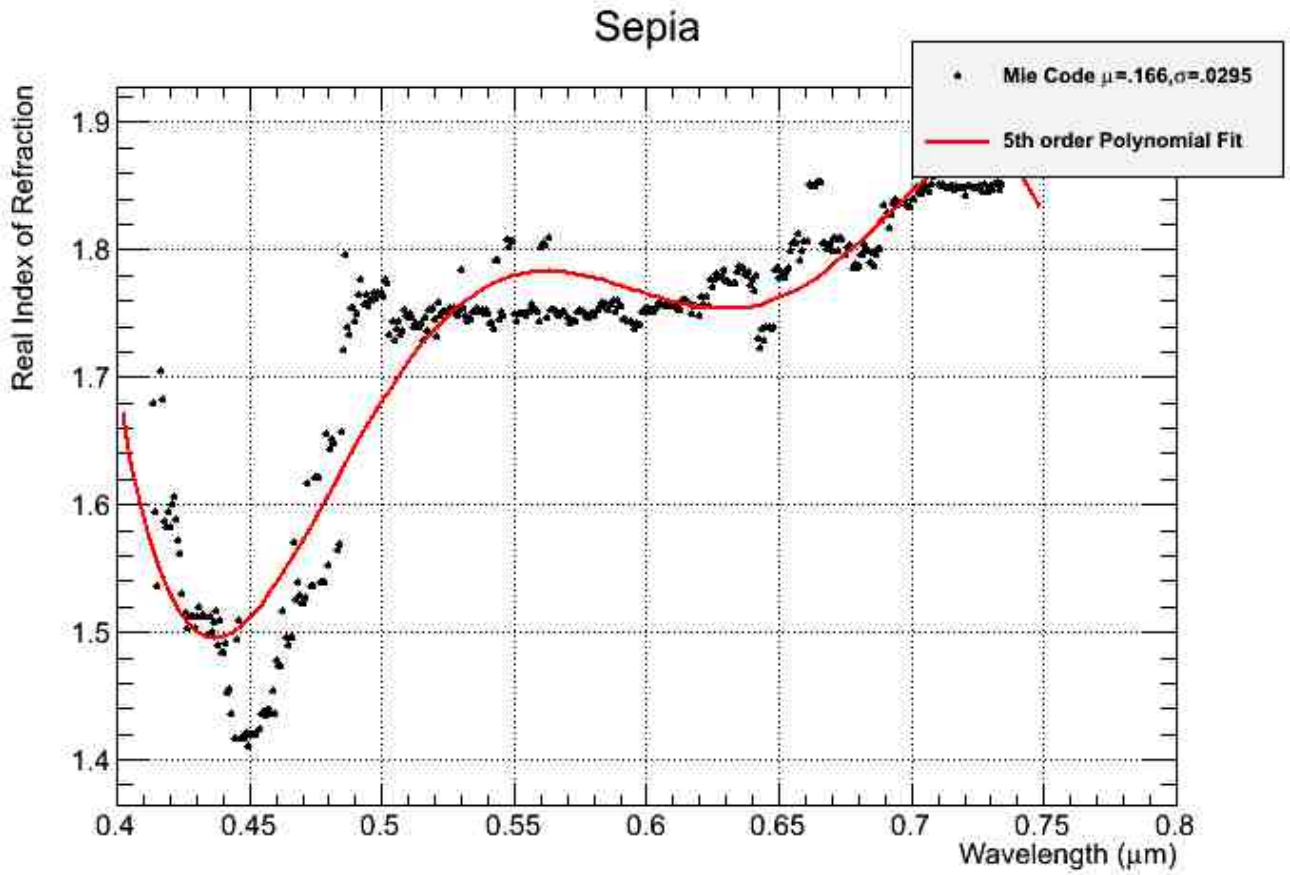

Fig. 12 The real index of refraction is being fit by a 5th order polynomial, the red line.

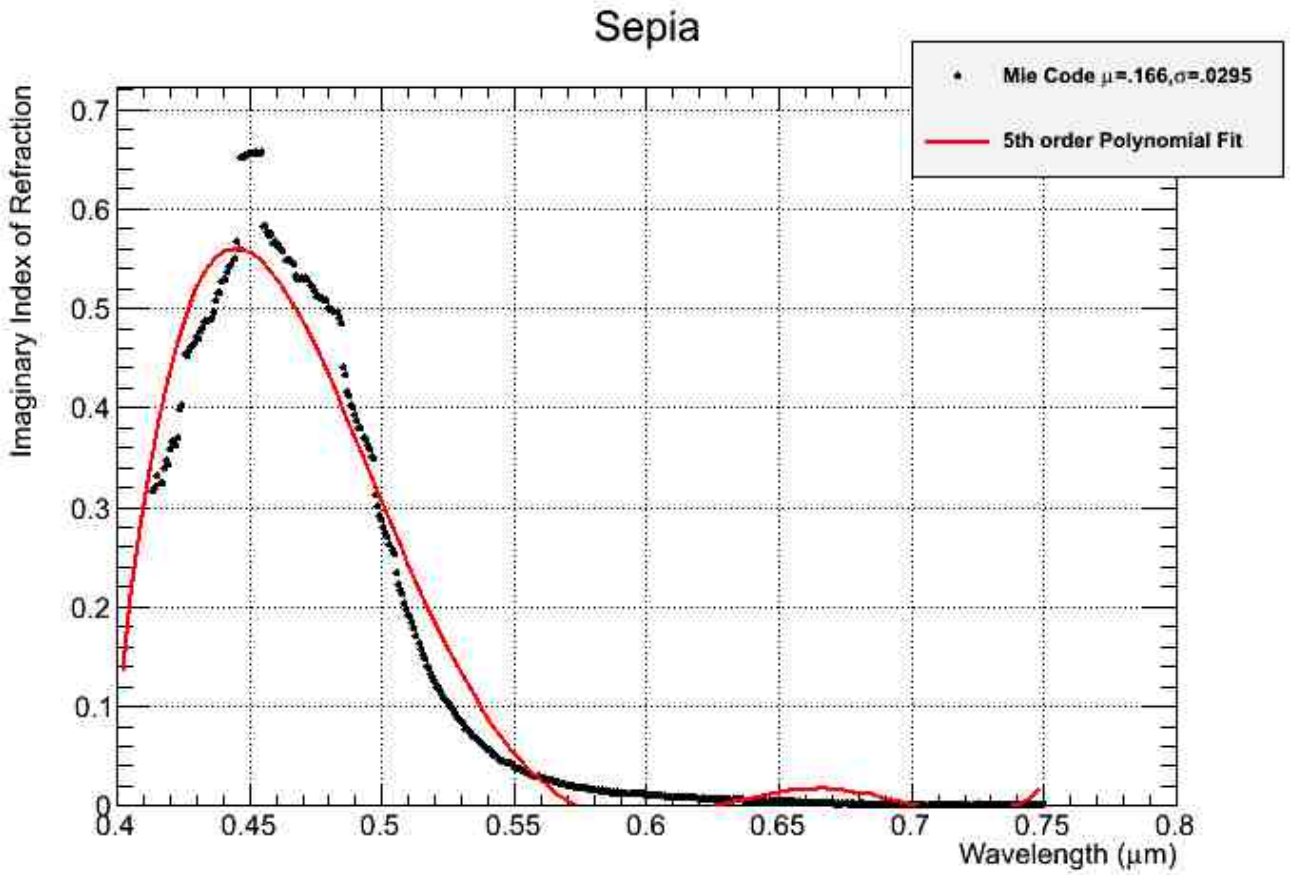

Fig. 13 The imaginary part of the index of refraction is being fit by a 5th order polynomial, red line.

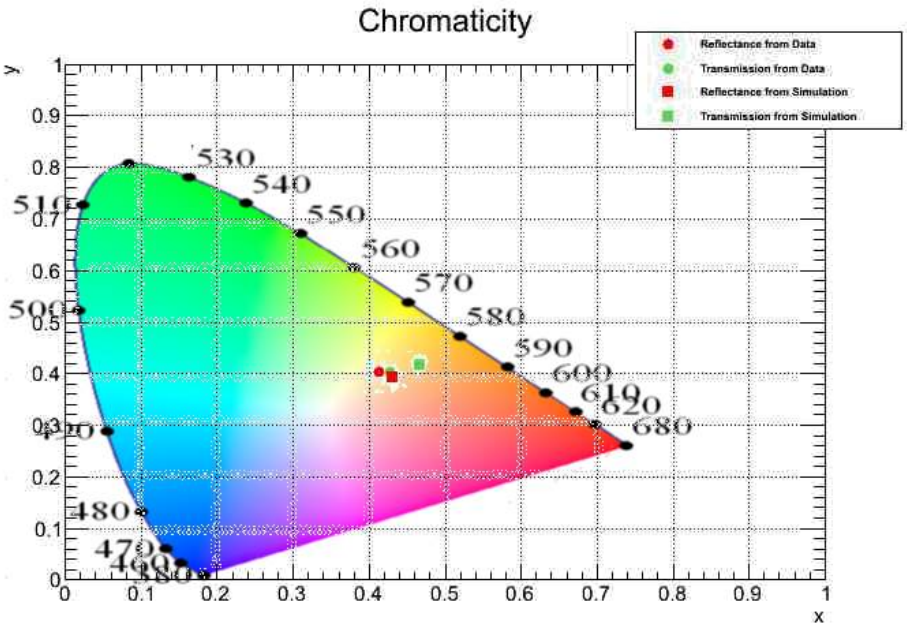

Fig. 14 The chromaticy plot shows that the simulated chromatophore is in the same color region as the actual chromatophore.

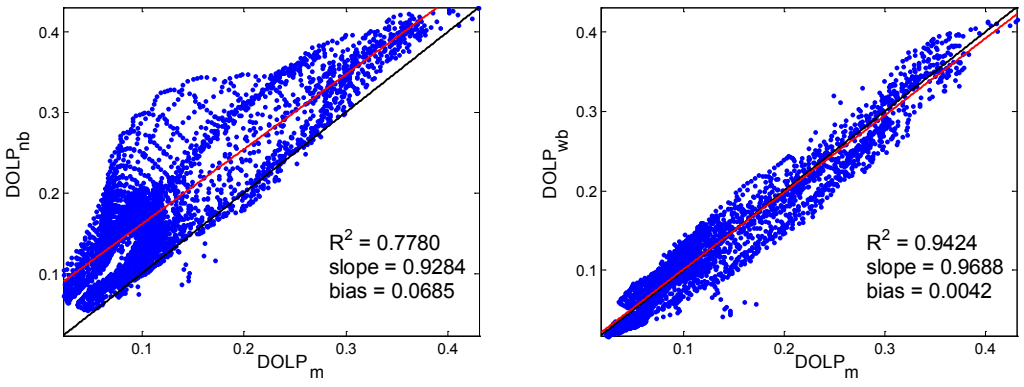

Fig.15 Measurements of the DoLP, denoted by the subscript "m," are scattered against simulations with no bottom ("nb") in panel (a) and against those with a bottom ("wb") in panel (b).

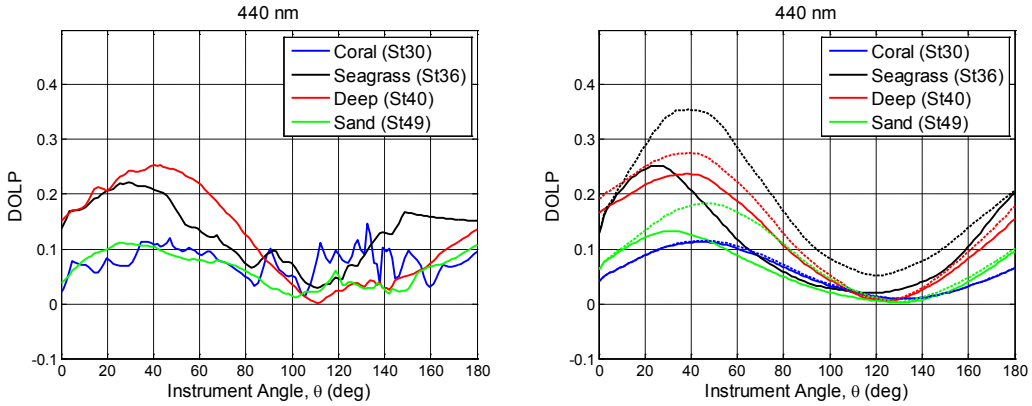

Fig. 16 DoLP as a function of instrument angle at three wavelengths at four studied sites. Left-hand panels: measurements. Right-hand panels: simulations; solid lines represent simulations with bottom effects, dashed lines represent simulations without bottom effects.

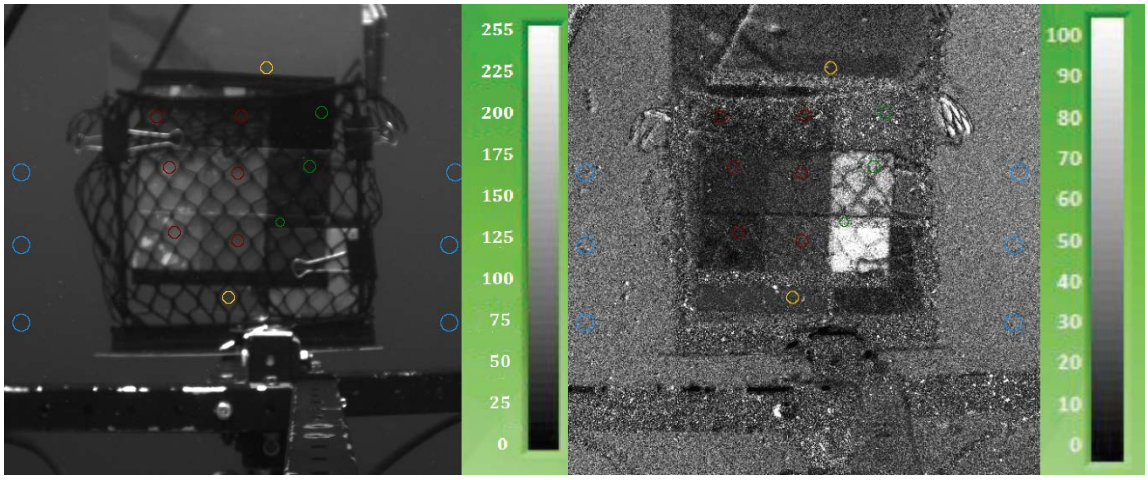

Fig. 17 The images of I component (scale in arbitrary units) and the DoLP (scale 0-100%) recorded by the camera at 90deg azimuth angle.

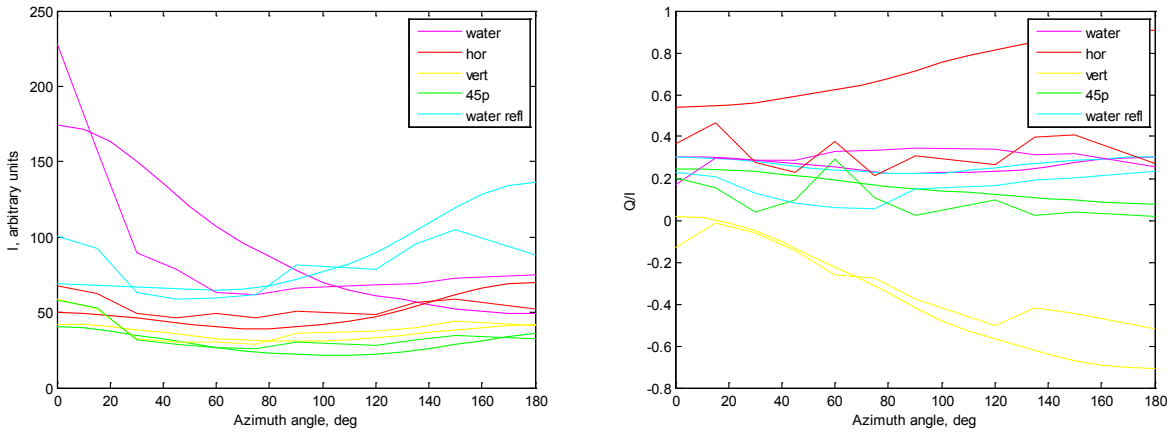

Fig. 18 The intensity I and Q/I measured by the camera and simulated by the model for water, mirror and target elements (solid lines – simulations, dashed lines – experiment).

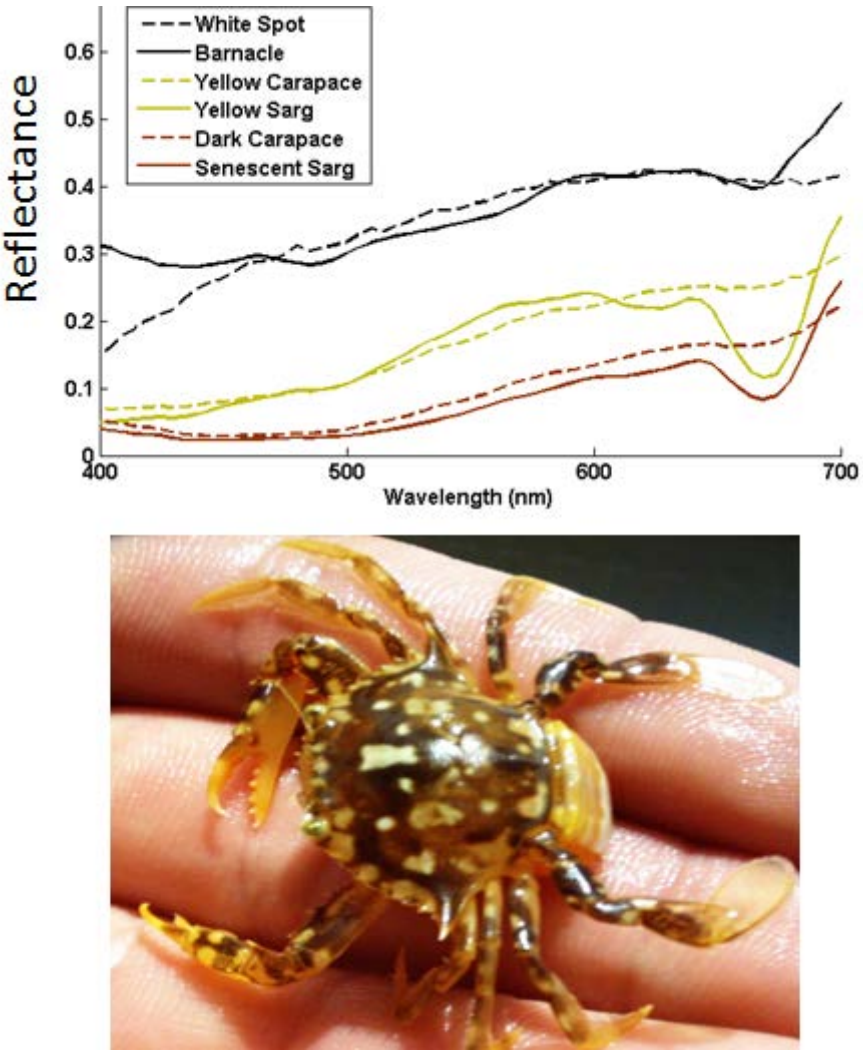

Figure 19. Hyperspectral imaging reveals specific components of Portunus sayi camouflage (light yellow, dark browns, central white spot) closely matching corresponding elements in algal habitat at visible wavelengths except the chlorophyll absorption band at 676 nm.

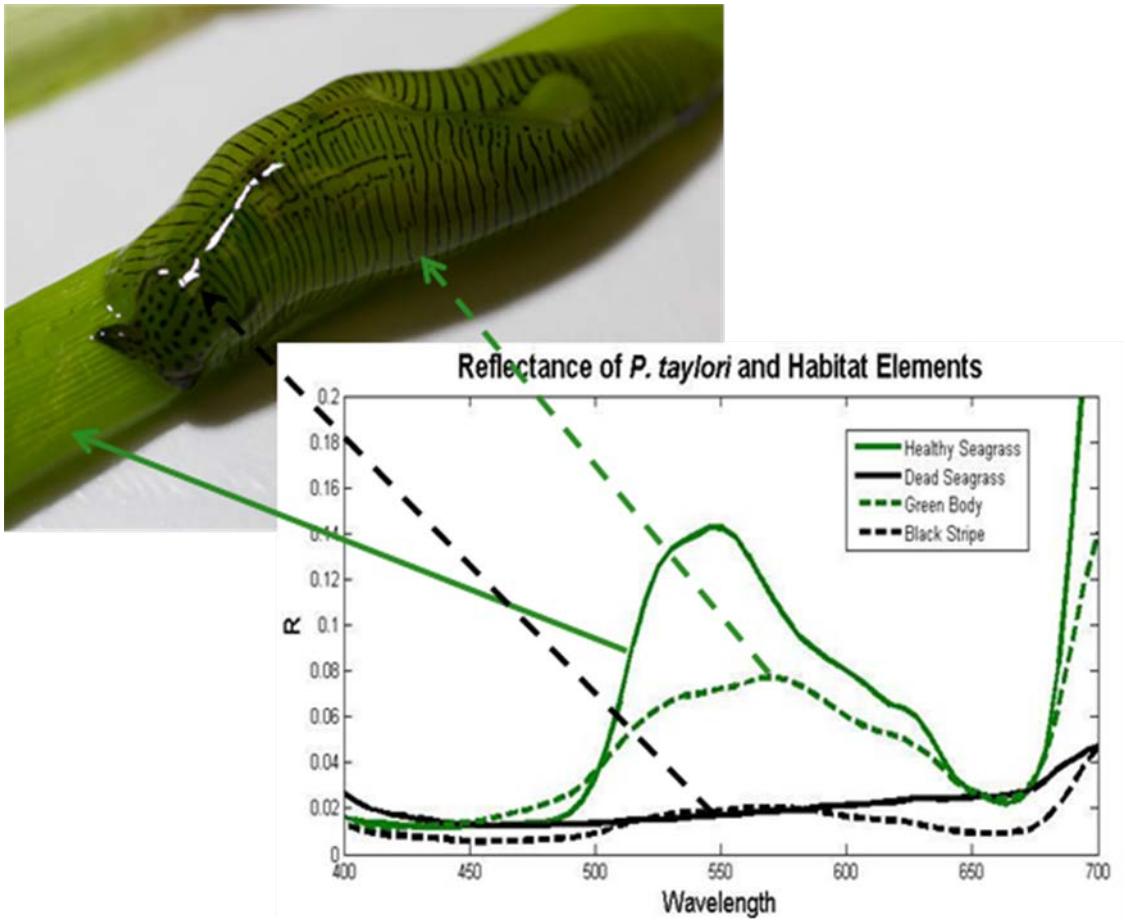

Figure 20. Hyperspectral imaging reveals Taylor's sea hare (Phyllaplysia taylori) matches the living and senescent eelgrass leaves at all wavelengths, including the region of chlorophyll absorption at 676 nm.

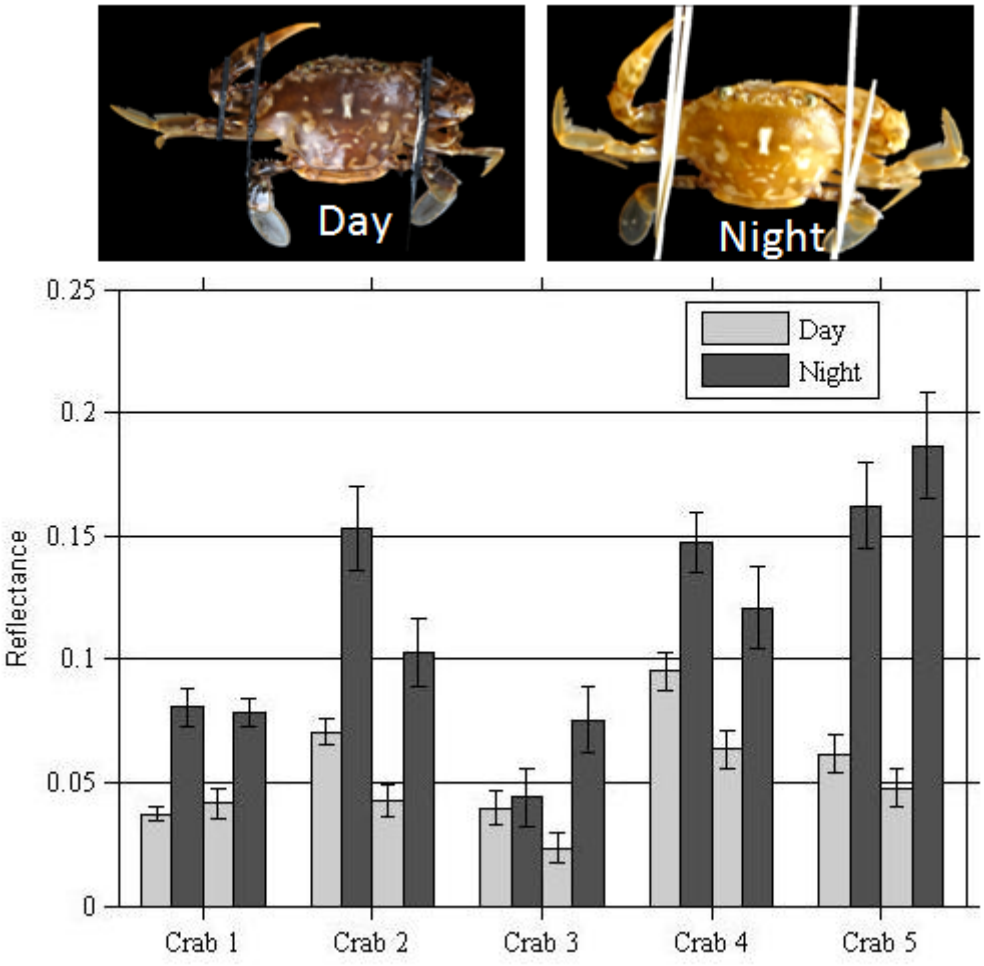

Figure 21. The crab Portunus sayi living in Sargassum habitats dynamically undergoes color change following the diel day and night light cycles through the use of chromatophores beneath the transparent carapace. Bars represent the average carapace reflectance at 550 nm for the five different crab individuals showing increased reflectance at night over two diel cycles.

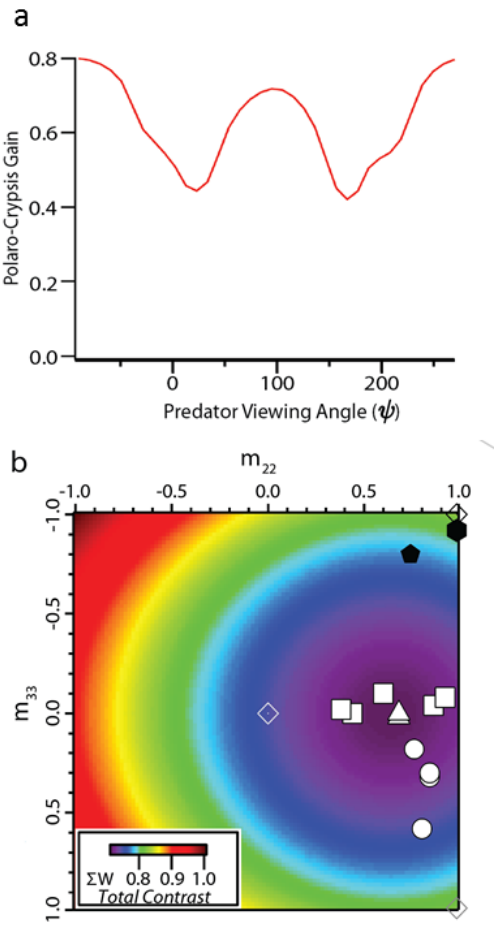

Figure 22. (a) With $\theta_s = 40°$, the percent crypsis gain is calculated between a vertical mirror and the lookdown Mueller matrix. The percent gain for fish-body pitch angle vs. observation angle is summed over a partial angular range of fish-body yaw angles ($|\varphi|>30°$) and predator-inclination angles ($\psi = -30°$ to $30°$), in 10° increments. The polaro-crypsis gain (PG) for the optimal fish-body pitch angle calculated as $PG = 100 \times (G_{Lookdown} - G_{verticalmirror}) / G_{verticalmirror}$ where G is defined as $G=W^{-1}$. (b) The pseudo-color image represents a 2D projection (m_{22} and m_{33} terms only, for other projections see Fig. S1) of the summation of the polarization contrast, W, over all θ, ψ, and φ angles in 10° increments with $\theta_s=40°$. The minimum value of the plot (purple) represents the optimal Mueller matrix for polarization crypsis with an unknown predator location. Triangle, circle, and square points are projected locations of the euthanized, microscope-measured, and live lookdowns, respectively, with each point representing an individual fish. The hexagon is the average of the polarization standard measurements, and the pentagon is the average of pinfish measurements. The black, off-white, and grey diamonds represent values for a vertical mirror, a completely-depolarizing mirror, and a mirror that acts as a half-wave plate, respectively (from Brady et al., 2012).

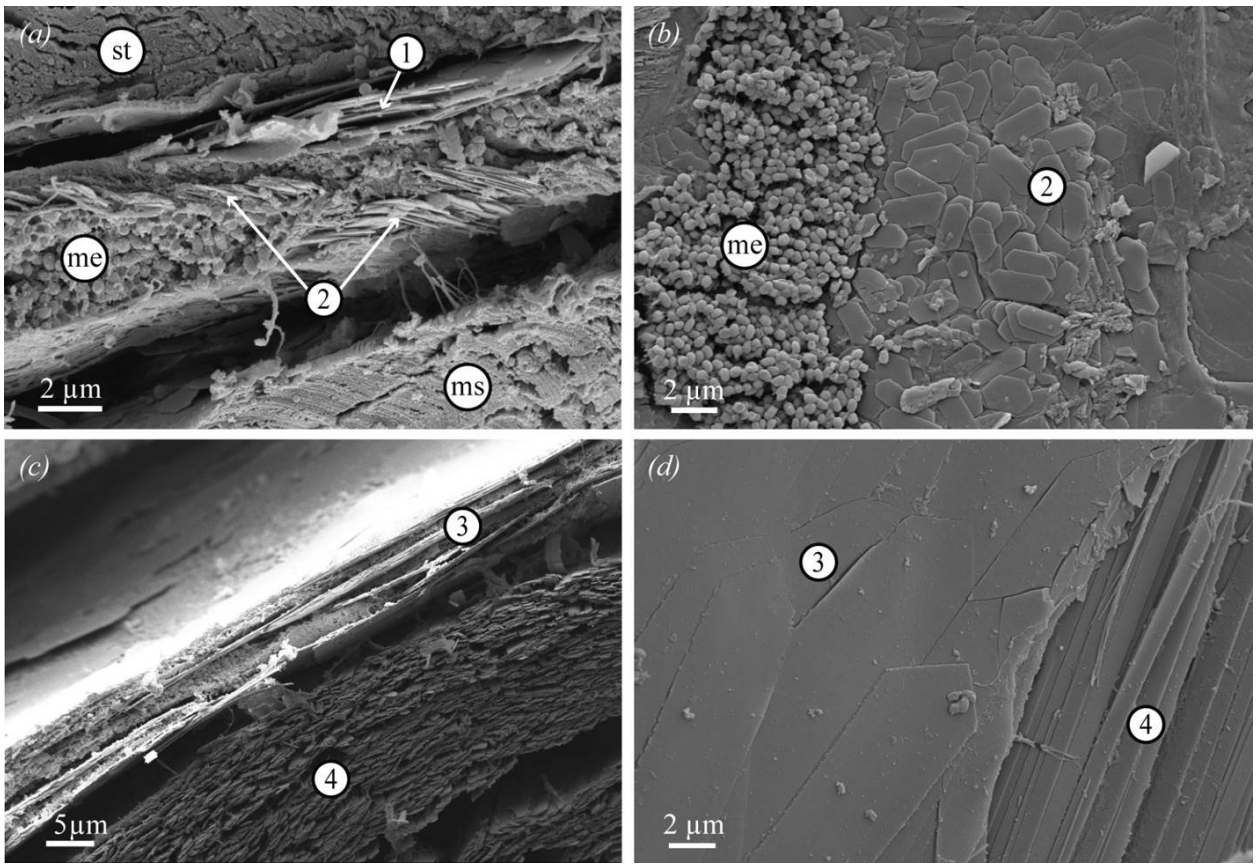

Figure 23. SEM images of the lookdown skin sections from the dorsolateral (a,b) and mid-lateral (c, d) flanks. (a) A cross-section shows Type 1 and Type 2 guanine platelets, melanosomes (me), stratum compactum (st), and muscle (ms) in the dorsolateral flank. (b) A parasagittal section of the dorsolateral skin shows melanosomes and Type 2 guanine platelets with various orientations. (c) A cross-section of the mid-lateral flank shows Type 3 and Type 4 guanine platelets. (d) A parasagittal section of the mid-lateral skin shows Type 3 and Type 4 guanine platelets.

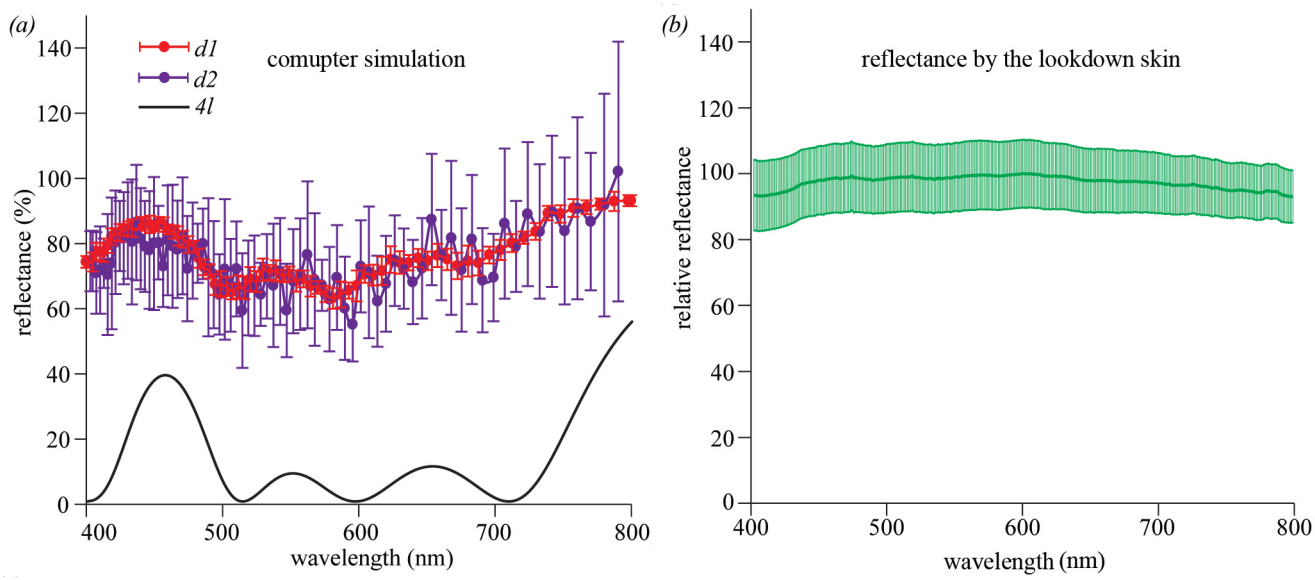

Figure 24. Broadband reflectance by the lookdown skin. (a) A 2D system (width =20μm, height = 70μm) that resembles the organization of the guanineplatelets in the lookdown skin was used for computer simulation. It consists of a random array of guanine platelet stacks. The widths of detectors d1 and d2 are 20 μm and 2 μm, respectively. Average reflectance from simulations of 10 randomly generated configurations. Error bars represent standard deviations. Reflectance detected by d1 (width =20 □m) is a relatively flat spectrum with small variations. Average reflectance detected by d2 (width = 2 □m) is similar to that by d1, but with much greater variations, indicating that great color variations between small areas. The black solid line shows the reflectance spectrum (by d1) of 4 layer platelets with an infinite radius. (b) Relative reflectance measured from the ventral flank of the lookdown. The dark green line is the average spectrum of nine measurements. The light green shade marks the standard deviations of the measurements (from Zhao et al., in review).

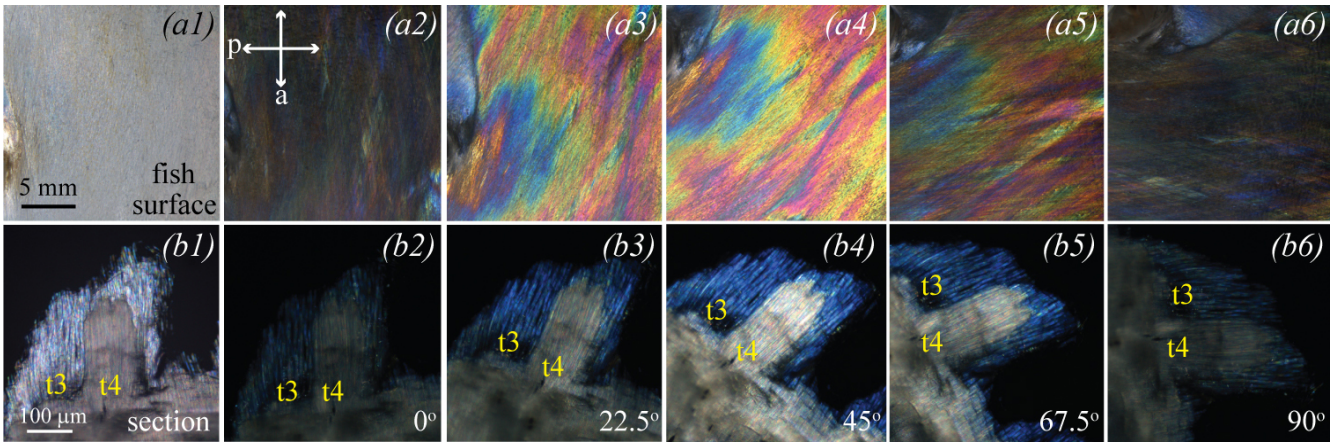

Figure 25. Polarization altering effects of birefringence of the intact lookdown skin surface (a1-a6) and the skin section (b1-b6) visualized with crossed polarization microscopy. (a1) An image of the mid-lateral flank of a juvenile lookdown was taken with unpolarized light. The anterior-posterior axis of the fish was horizontal with the fish head on the left. (a2-a6) Images of the same view as in (a1) were taken with crossed polarizers as the fish was rotated from the horizontal position (0 degree) clockwise by 22.5, and 45, 67.5, or 90 degrees, respectively. The maximum effect was observed as the fish was rotated by 45^{o} (a4). The orientations of the polarizer (p) and analyzer (a) are indicated by the arrows in (a2). (b1) An image of a parasagittal section of the mid-lateral skin of an adult lookdown was taken with unpolarized light as the long axes of the platelets were aligned with the analyzer. (b2-b6) Images of the same view as in (b1) were taken with crossed polarizers as the tissue section was rotated from its original position (0 degree) clockwise by 22.5, and 45, 67.5, or 90 degrees, respectively. The long axes of Type 3 (t3) and Type 4 (t4) platelets were in the same orientation. They both had minimum visibility when their long axes were in vertical or horizontal position while the maximum visibility was reached as the section was rotated by 45^{o}. The Type 3 platelets appeared blue while Type 4 plateletes were muti-colored at high magnification and appeared nearly white at low magnification (b4) (from Zhao et al., in review).

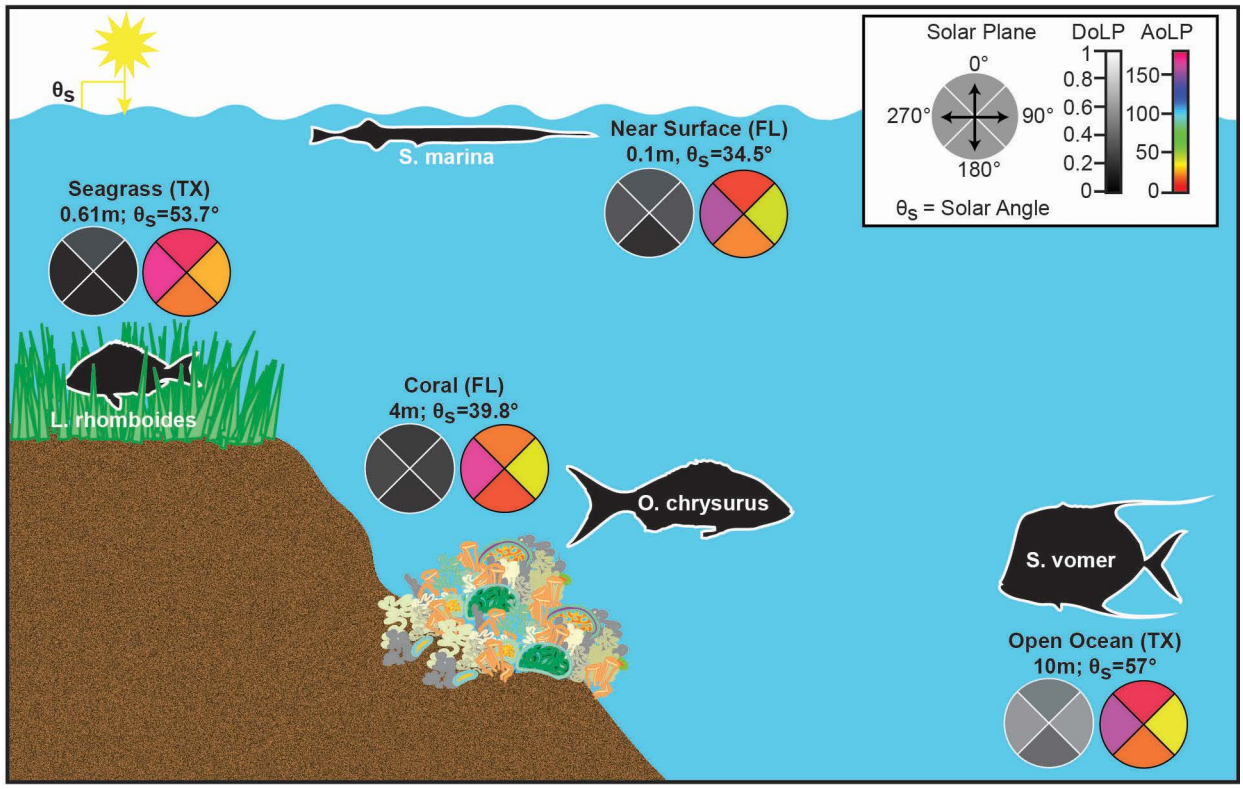

Figure 26. Water column polarization measurements for seagrass beds, coastal/reef and open-ocean. Each location represents habitats for different species: Selene vomer (lookdowns) reside in the open ocean; Strongylura marina (Atlantic needlefish) are near-surface fish; Ocyurus chrsurus (yellowtail snapper) inhabit reef/coral structures; and Lagodon rhomboides (pinfish) occupy shallow seagrass habitats. Polarized measures of both fish and water column were recorded using two videopolarimeters. Solar Angle refers to the angle of the sun in relation to the surface of the water. Solar Plane is the azimuthal viewing angle, i.e. the angle underwater as an object rotates in a circle around a central axis. Here, the camera is horizontally rotating around its central axis to record the polarized field looking directly into the sun (0˚), 90˚, 180˚, and 270˚ away from the sun (Data from Ruddick et al., in review).

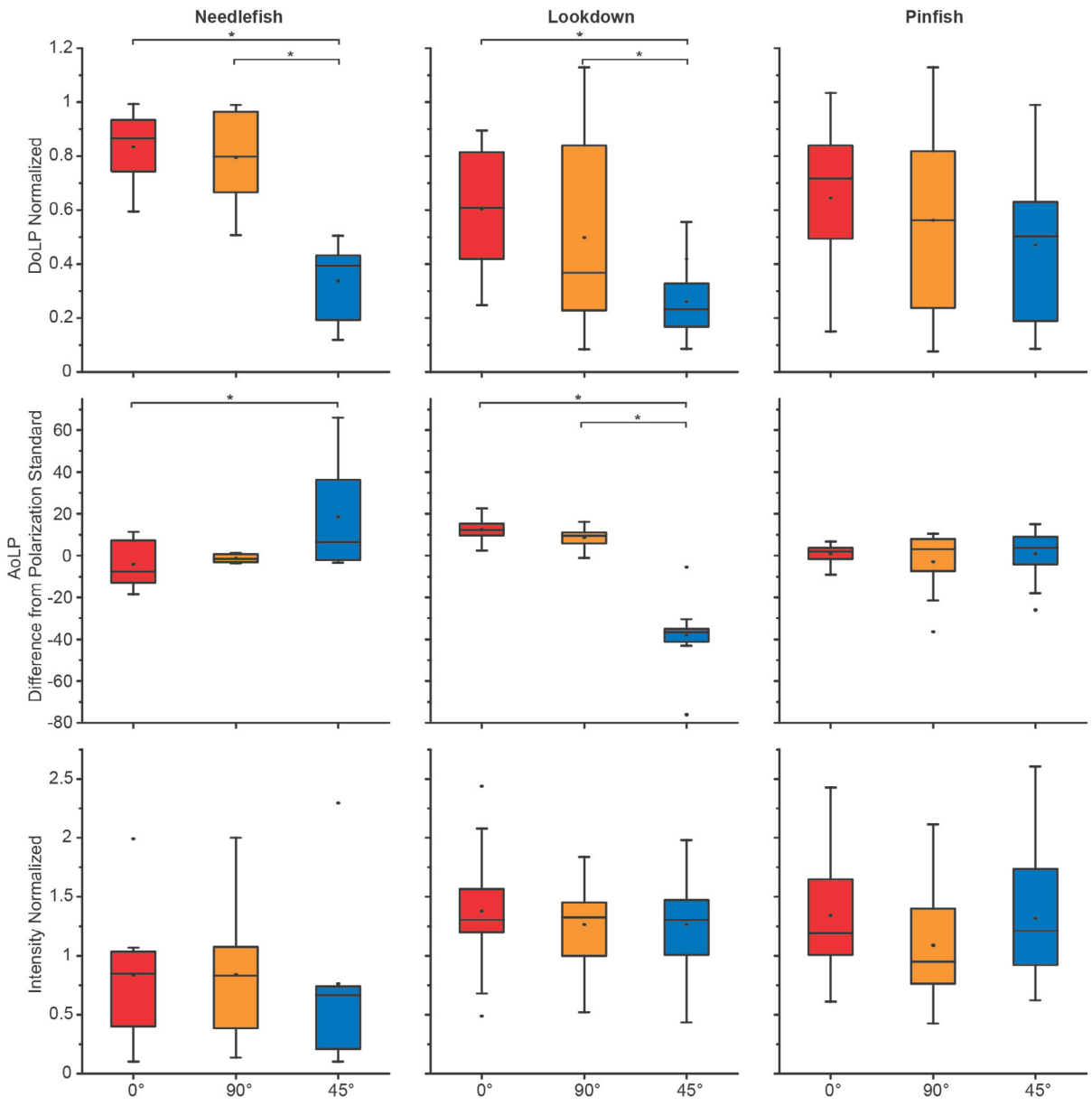

Figure 27. Polarized reflectance for three species (Atlantic needlefish (n=8), lookdowns (n=24), pinfish (n=23)). One-way ANOVAs indicate within species significance for DoLP for needlefish and lookdowns, but not pinfish (needlefish and lookdowns: p<0.00001). Tukey post-hoc tests show significant difference for the 0° to 45° and 90° to 45° comparisons for needlefish and lookdowns. One-way ANOVAs also result in significance for AoLP reflectance for needlefish and lookdowns (needlefish: p=0.02, lookdowns: p<0.00001). Tukey-Kramer post-hoc shows significance between 0° and 45° for needlefish and lookdowns and also between 90° and 45° for lookdowns. However, circular ANOVA did not show significance for needlefish (p=0.06). This indicates species difference in polarized reflectance (Data from Ruddick et al., in review).

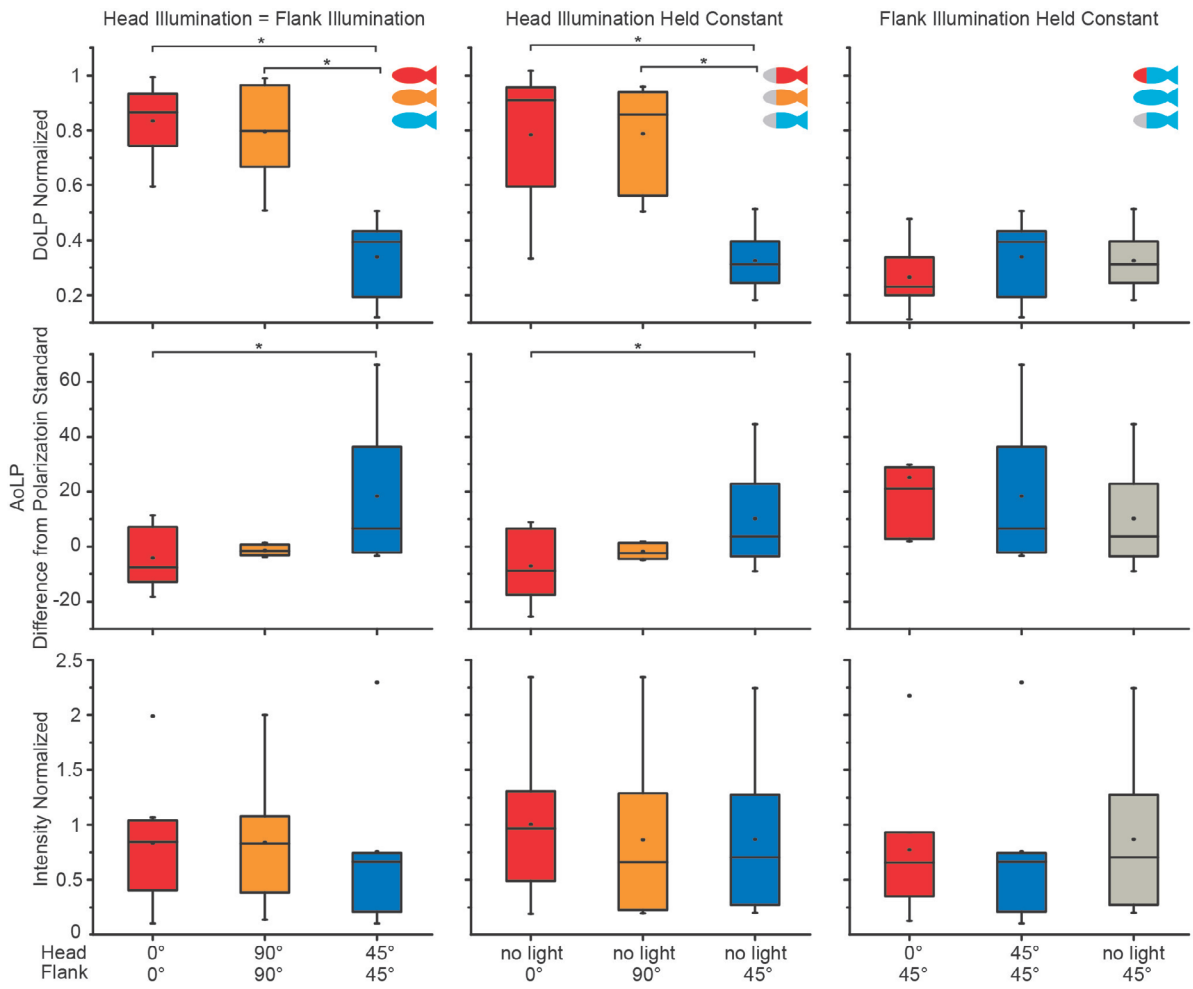

Figure 28. Atlantic needlefish (n=8) polarized reflectance measurements. The left column represents data seen in Figure 3 where the head and flank incident polarized illumination angle are the same. DoLP is significantly different ($F(2,20)=3.49$, $p<0.00001$) with Tukey-Kramer post-hoc tests show significant difference for the 0° to 45° and 90° to 45° comparisons. The middle column (fish head/visual system illumination does not change - flank illumination changes), illustrates the same pattern of significance as seen as in the left column for DoLP. When illumination to the visual system changes but flank illumination stays constant, no significant differences between flank reflectance is found ($F(2,20)=3.49$, $p=0.46$). If head and flank illumination is the same, AoLP reflectance is significantly different between 0° and 45° ($F(2,20)=3.46$, $p=0.02$; Tukey-Kramer post-hoc), but circular statistics reveal non-significance ($F(2,20)=3.20$, $p=0.06$). Statistics for the middle column (flank changes, head does not) also reveal significant differences between conditions ($F(2,20)=3.49$, $p=0.05$) with Tukey-Kramer post-hoc showing that the 0° to 45° are significantly different. Again, circular statistics does not show a difference in this comparison ($F(2,20)=2.95$, $p=0.08$). The right column compares conditions when the head/visual system illumination changes, but the flank illumination does not. No significance is seen indicating that polarized reflectance is based more on mechanisms at the skin/flank level than at the visual level (Data from Ruddick et al., in review).

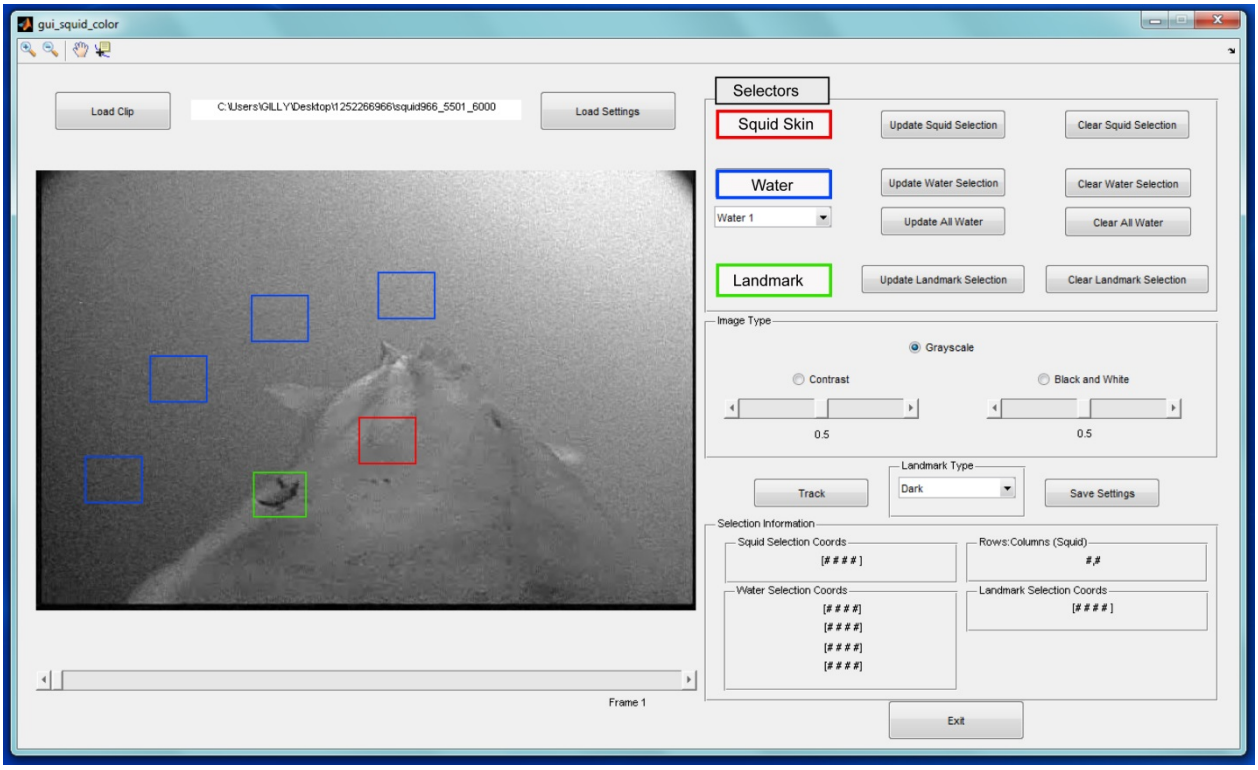

Figure 29. Squid Skin Graphical User Interface for automated analysis of chromogenic behaviors of Dosidicus gigas based on Crittercam video clips. The dorsal surface of the camera-bearing squid is visible. A Landmark selector (Green button) enables positioning a perimeter around an anatomical mark (green square) that can be used to track movements of the squid's head from frame to frame. A Squid Skin selector (red button) defines an area of skin in which changes in skin color can be analyzed over time. These data are corrected for movements of the squid's head in the frame by linking the spatial.

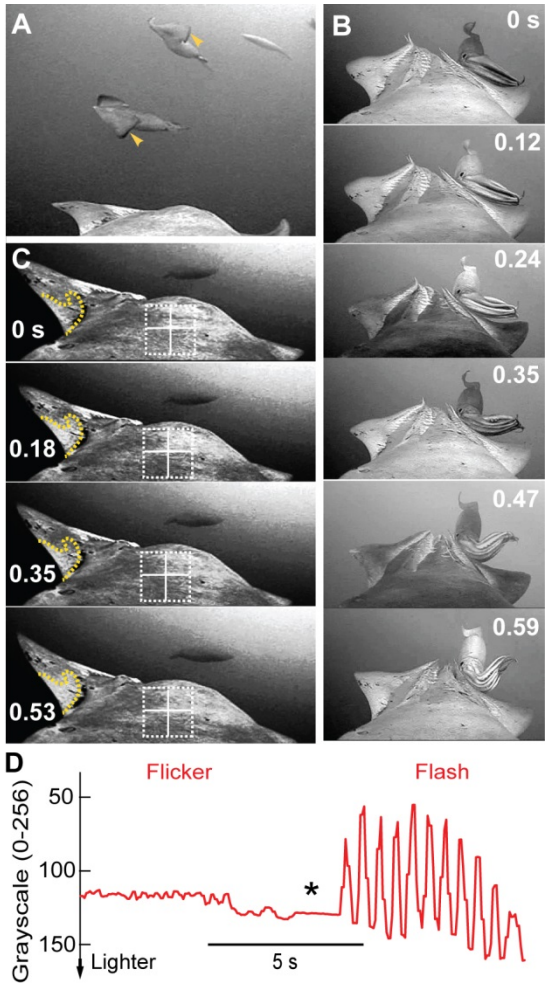

Figure 30. Chromogenic behavior in Dosidicus at a depth of ~ 20 m recorded with Crittercam in the Gulf of California analyzed using the Squid Skin GUI. The dorsal surface of the camera-bearing squid is visible in each video frame (17 Hz). (A) Two squid displaying the "fin –stripe" pattern (arrows). (B) Bidirectional flashing with an encountered squid (every other frame displayed). (C) Flickering (every fifth frame displayed) is best visualized by examining activity within specific outlines (yellow dots on left arm-keel or white grid on head). (D) Time-series of chromatophore activity on the surface of the head (averaged over dotted square) showing the temporal characteristics and comparative amplitudes of flickering and flashing. The asterisk denotes a cessation of chromatophore activity between flickering and a flashing episode.

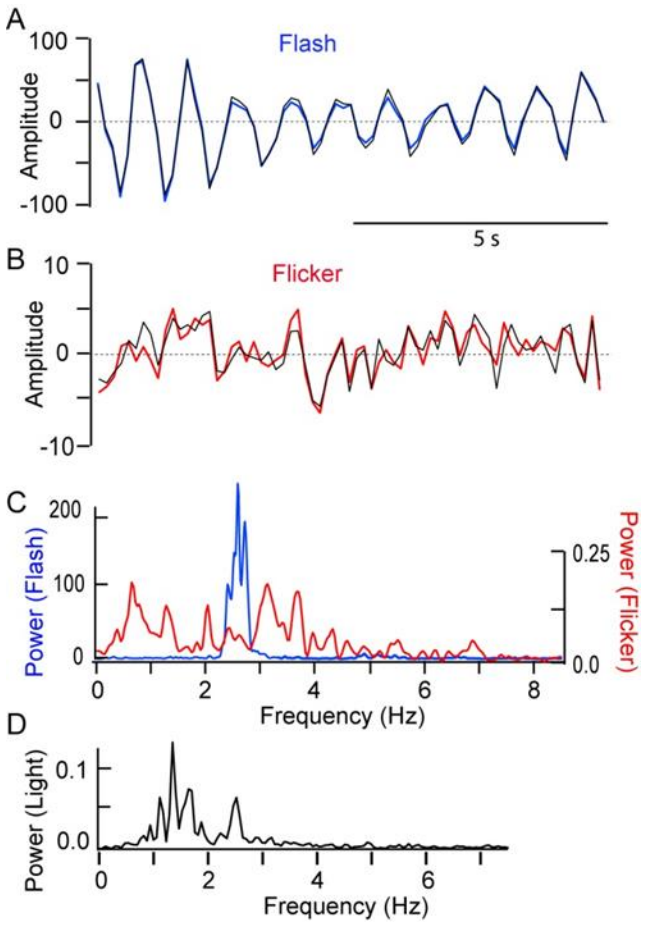

Figure 31. Spectral analysis of chromogenic behavior using the Squid Skin GUI.

A. Time course of flashing in two adjacent areas corresponding to the bottom left quadrant in Fig. 2B (blue trace) and bottom right quadrant (black trace). Raw data were high-pass filtered (0.5 Hz cutoff) and fit with a sloping baseline to the resultant.

B. Time course of flickering after processing the raw data as described above. Bottom left quadrant is the black trace; bottom right is red.

C. Power spectra for 30 sec of continuous flashing (blue) and flickering (red) generated by Fast Fourier Transform. Flashing has a prominent peak at ~2.6 Hz. Flickering has less well-defined peaks, but spectral structure is evident between 1 and 4 Hz.

D. Spectral data for variation in natural light-field recorded independently in the Gulf of California. Spectral structure between 1-3 Hz is evident. Light was recorded at 6.75 m depth; displayed trace is the average of measurements at 410, 433, 488, 532, 610 and 670 nm. Light field data were provided by M. Darecki and D. Stramski.

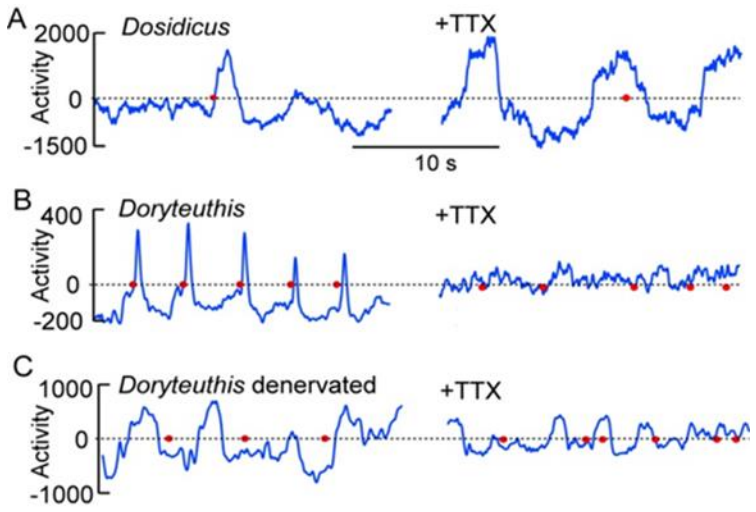

Figure 32. Chromatophore activity and effect of TTX. Stimuli were delivered at indicated times (solid circles on dotted baseline). The left side of each panel is in seawater; the right side is in 100 nM TTX. Activity (number of expanded chromatophores in a 1 cm x 1cm field) was measured as the deviation from a mean value during a 60 s period preceding the illustrated segments. Video frames were converted to BW and contrast-enhanced. Open (B) chromatophores were assigned a value of 1; background (W) was 0. 1. Chromatophore expansion is an upward deflection from the baseline. (A) Dosidicus: the first stimulus (1 ms duration) generated a combined fast and slow response. The second stimulus was subthreshold. TTX abolished stimulated activity but did not block spontaneous activity (Gulf of California, RV New Horizon, June, 2011). (B) Doryteuthis: Stimulation (0.5 ms duration) produced rapid expansion. TTX blocked this activity (Hopkins Marine Station, June, 2012). (C) Doryteuthis denervated: Spontaneous waves occurred in the denervated field (1 week post-op); electrical stimuli were ineffective. Waves persisted in TTX (HMS, June, 2012).

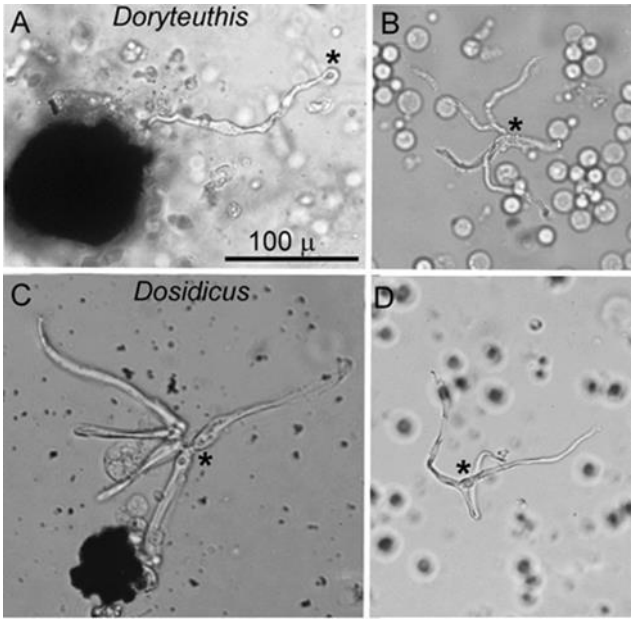

Figure 33. Living elements of the chromatophore system in primary culture from Doryteuthis (A,B; HMS, May, 2012) and Dosidicus (C,D; HMS, Oct. 2012). Small pieces of skin were treated with non-specific protease (Type XIV, Sigma) for 1 hour at 20°C and mechanically dissociated by trituration. Cells were maintained in L15 medium (pH 7.8) with supplemented salts to match seawater (except for no added $CaCl_2$) at 15 °C overnight before photographing (20X water immersion objective). (A) Radial muscle fiber adjacent to a chromatophore pigment sac. The apparent nucleus (asterisk) suggests this proximity may be fortuitous. (B) Multipolar cell. Putative cell body with nucleus is labeled with asterisk. (C) An incomplete ring of radial muscle fibers that remained attached to one another after separation from the pigment sac. Asterisk marks nuclear ends of fibers. (D) Multipolar cell with putative cell body indicated by asterisk.

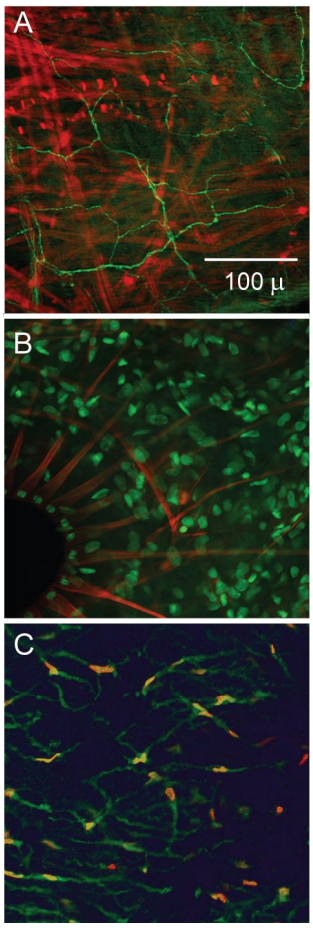

Figure 34. Fluorescently labeled elements in skin of Doryteuthis opalescens. (A) Superimposed images of actin (red; Alexa Fluor 488 phalloidin) and 5HT (green; rabbit anti-5HT, Sigma and Alexa Fluor 546 secondary antibody) labeling. Presumptive serotonergic axons approach muscle fibers. (B) Radial muscle fibers of a chromatophore at lower left are labeled for actin (red) as in panel A. DAPI (green) was used to stain DNA in nuclei of all cells. Nuclei of the radial muscle fibers form a ring around the pigment granule. Many other unidentified nuclei are present. (C) Cell bodies of presumptive serotonergic processes (green; anti-5HT) with nuclei labeled with DAPI (orange). These processes appear to form a network of nucleated cells that are distinct from the axons labeled in panel A. They appear to be similar to the multipolar cells describe in Fig. WG5. Methods: Skin was fixed in 4% paraformaldehyde in Ca-free artificial sea water (ASW): (in mM) 480 NaCl, 10 KCl, 20 $MgCl_2$, 20 $MgS0_4$, 10 Hepes (pH 7.8) for 4 hours at room temperature, washed overnight in Ca-free ASW and then in standard PBS with 0.1% Na azide.. Incubation in primary antibody (anti-5HT) was for 3 hours and in secondary antibody for 1 hour. Whole-mounts of flat pieces of intact skin were cleared in glycerol for imaging. Panel A was made using a Zeiss AxioImager Z1 microscope with a 20x objective and Apotome and Axiovision software that allows analysis of optical sections 1-2 um thick. This work was done with C. Lowe at Hopkins Maine Station (June 2012). Panels B and C was acquired with a confocal microscope using the DAPI laser setting and a 546 nm laser for 5HT and 20 x objective in a multiuser confocal facility at HMS in July 2013.

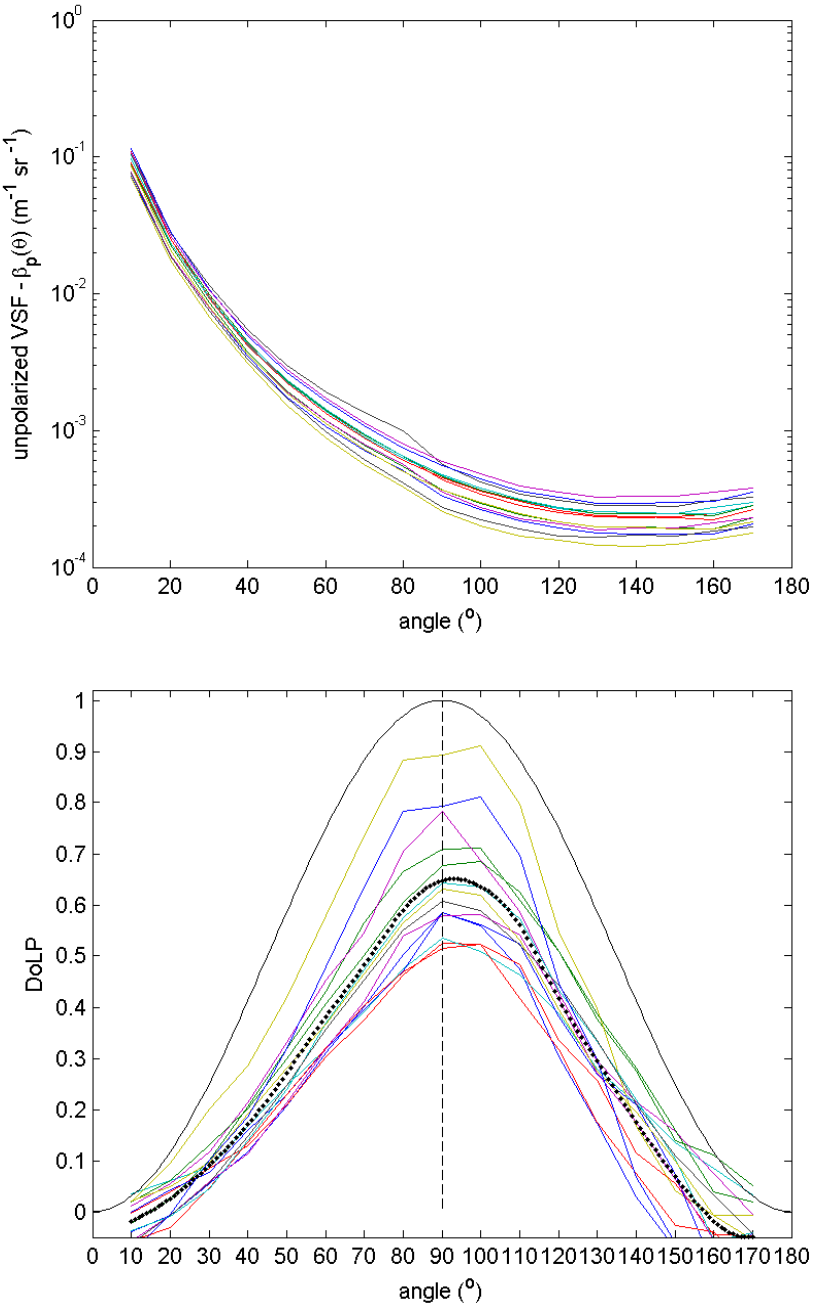

Figure 35a (top panel) - The average unpolarized VSFs collected for each station during the 2012 field experiment. Figure 35b (bottom panel) - The average DoLPs collected for each station during the 2012 field experiment. The dotted black line represents the average of all stations. The solid black line represents the Rayleigh ideal.

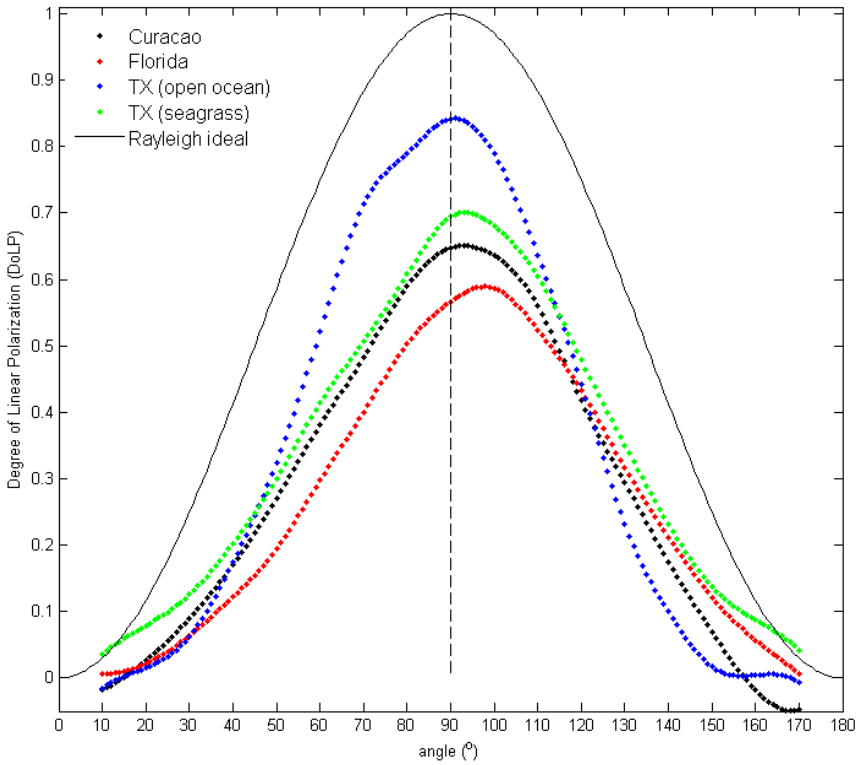

Figure 36. The average water column DoLP collected at each MURI field location. The solid black line represents the Rayleigh ideal. As the DoLP decreases in different environments, the peak gets further displaced to larger angles from the 90° Rayleigh ideal.